

Extrasolar enigmas: from disintegrating exoplanets to exoasteroids

Jan Budaj, Petr Kabath and Enric Palle

Abstract Thousands of transiting exoplanets have been discovered to date, thanks in great part to the *Kepler* space mission. As in all populations, and certainly in the case of exoplanets, one finds unique objects with distinct characteristics. Here we will describe the properties and behaviour of a small group of ‘disintegrating’ exoplanets discovered over the last few years (KIC 12557548b, K2-22b, and others). They evaporate, lose mass unraveling their naked cores, produce spectacular dusty comet-like tails, and feature highly variable asymmetric transits. Apart from these exoplanets, there is observational evidence for even smaller ‘exo-’objects orbiting other stars: exoasteroids and exocomets. Most probably, such objects are also behind the mystery of Boyajian’s star. Ongoing and upcoming space missions such as *TESS* and *PLATO* will hopefully discover more objects of this kind, and a new era of the exploration of small extrasolar systems bodies will be upon us.

1 Introduction

The exoplanet science discoveries kicked-in after 1992-1995 when the first exoplanets were discovered [1] first around a pulsar and then a hot Jupiter around a solar type star 51 Peg [2]. The exoplanet 51 Peg b was detected from observations of radial

Jan Budaj

Astronomical Institute, Slovak Academy of Sciences, 05960 Tatranska Lomnica, Slovakia, e-mail: budaj@ta3.sk

Peter Kabath

Astronomical Institute of Czech Academy of Sciences, Fričova 298, 25165, Ondřejov, Czech Republic e-mail: petr.kabath@asu.cas.cz

Enric Palle

Instituto de Astrofísica de Canarias, Calle Vía Láctea, s/n, 38205 San Cristóbal de La Laguna, Santa Cruz de Tenerife, Spain e-mail: epalle@iac.es

velocities (‘RV’) from the ground with a 1.92-m telescope located at Observatoire de Haute Provence.

Later hundreds of exoplanets were discovered using the radial velocity method. In 2000, the first *transiting* exoplanet HD209458b, again a Jupiter-sized planet in a close-in orbit, was detected [3]. New automated ground-based projects to detect transiting exoplanets were started in the first decade of 21st century. The most successful of such projects to date is the WASP survey¹ which has discovered about 200 transiting planets (April 2019), and there are a number of other successful ground-based exoplanet surveys as well, such as HAT [4] or KELT [5].

A real breakthrough came with the launch of the CoRoT space mission in 2006. The CoRoT satellite was a french-led ESA mission carrying a 28-cm aperture telescope equipped with 4 CCD detectors dedicated to asteroseismology and exoplanetary transit detections [6]. The CoRoT mission was terminated in 2013 and it reported 33 exoplanets which are all fully characterized and thus we know both their masses and radii.

In 2009 a very successful NASA space mission *Kepler* was launched carrying a telescope with a mirror of 1.4-m with a large array of CCD detectors [7]. *Kepler*, and later its continuation *K2* mission, discovered during their lifetimes from 2009 until 2018 about 4000 transiting exoplanets. *Kepler/K2* photometric data likely still contain many more new planetary candidates. However, only a few hundreds of the *Kepler/K2* planets have been fully characterized, so that we know their masses and radii. This fact is due to the relative faintness of the *Kepler/K2* targets and the difficulty of carrying out ground-based follow-up spectroscopic RV observations. However, despite these limitations, *Kepler/K2* was able to deliver extremely interesting candidates, among them low mass and rocky planets in the habitable zone such as Kepler-62f [8], ultra-short period planets such as Kepler-78b [9], and multiple planetary systems [10]. Also, new types of objects such as Boyajian’s star [11] and ‘disintegrating’ planets [12] were found with *Kepler/K2*.

In the following text, we will focus on the physics behind the more recently discovered enigmatic objects such as disintegrating and evaporating planets. A significant number of such objects are also expected to be discovered with the most recent and upcoming missions like *TESS* and later *PLATO*. Before discussing the physics of the disintegrating objects, we briefly introduce the observing strategies which led to the discoveries of these interesting types of exo-objects.

In Section 2 we describe the methods and observing strategies used to discover or characterize these ‘dusty objects’. Section 3 contains a crash course on the dust properties which are important to understand the content of this chapter. Sections 4, 5 describe the most interesting disintegrating exoplanets and minor bodies in exoplanetary systems. The special case of Boyajian’s star is discussed in the Section 6. Finally, Section 7 deals with ongoing and future space missions which may bring new fascinating discoveries and open a new era in the study of these extrasolar objects. For a reference, another recent review of disintegrating exoplanets can be found in [13].

¹ <http://www.superwasp.org>

2 Observing methods and strategies

The most successful methods of exoplanet detection are the transit and radial velocity measurements. Both methods benefit from their combination, and, in general, all planets detected by the transit method need follow-up radial velocity measurements for mass determination. Therefore, all exoplanetary transit space missions try to ensure that the targets in their prime sample can be followed-up spectroscopically from the ground.

2.1 Radial velocities (RV)

The method of discovering and characterizing exoplanets by precise radial velocity measurements is based on Kepler's laws. If the system consists of a star and a planet, these orbit around their common center of mass causing the star to move toward and away from the observer with a given radial velocity that is a function of the mass of the planet. Detailed derivations of the expression for the semi-amplitude K of the radial velocity curve can be found in numerous publications [14, 15]; therefore, we limit ourselves here to only presenting the final expression for the semi-amplitude of the radial velocity curve K :

$$K = \frac{1}{\sqrt{1-e^2}} \left(\frac{2\pi G}{P_{\text{orb}}} \right)^{1/3} \frac{M_{\text{plan}} \sin i}{(M_{\text{star}} + M_{\text{plan}})^{2/3}} \quad (1)$$

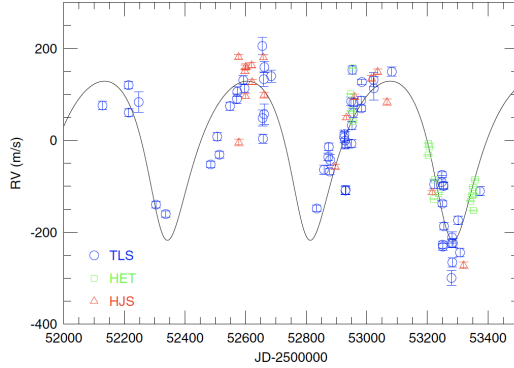
where G is the gravitational constant, P_{orb} the orbital period, M_{star} the stellar mass, M_{plan} the planetary mass, i planetary orbital inclination angle, and e the eccentricity of the planetary orbit. As can be seen from the above equation, the resulting radial velocity and the corresponding semi-amplitude K can be obtained from the observed spectroscopic time series that adequately samples the orbital phases. However, this method can not provide a determination of the inclination, i , of the planetary orbital plane. Therefore, the value of planetary mass M_{plan} obtained from the RV measurements is only a lower limit since the value of i is unknown without making use of the photometric transit data. One example of an RV curve is illustrated in Fig. 1

The typical radial velocity semi-amplitude of a large gas planet is of order of tens to hundreds of m/s. On the other hand a typical radial velocity signature of an Earth-sized planet can be as low as few cm/s.

2.2 The transit method

If a planet passes in front of the stellar disc along observer's line of sight, then one can observe a periodic dimming of the stellar light, i.e., a transit. Typically a photometric time series with good sampling is obtained a few hours before, then

Fig. 1 Figure shows a typical RV curve of a gas planet obtained with various telescopes around the globe. Figure Credit: [16] DOI:10.1051/0004-6361:20052850, reproduced with permission © ESO.



during the transit, and finally a few hours after the transit ends. The basics of the method have been described in great detail elsewhere [17]. Here we limit ourselves to expressing the transit depth, δ , as:

$$\delta \propto \frac{\Delta F}{F} = \frac{R_{\text{plan}}^2}{R_{\text{star}}^2} \quad (2)$$

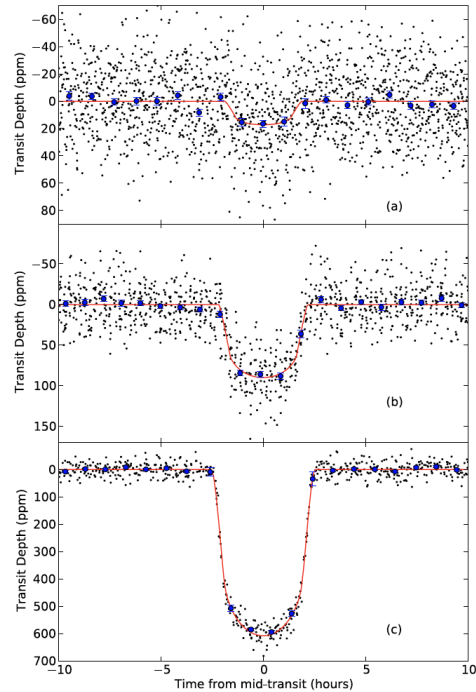
where ΔF is the observed change of flux during a transit, F the flux of the star, R_{plan} the planetary radius, and R_{star} the stellar radius. An advantage of this method is that it can be used to determine the inclination of the planet's orbital plane if the stellar parameters of the host star are known. It is clear that the photometric transit method needs to be combined with spectroscopic observations of a given system in order to fully characterize the exoplanet.

The detection of hot-Jupiters can be accomplished even with small-aperture telescopes as the typical transit depth, δ , due to a transit of a hot-Jupiter is a few percent of the stellar flux for a main sequence dwarf star. However, the detection of Earth-sized planets requires ultra-precise photometry, typically measured in parts per million ('ppm'). CoRoT-7b was the first example of a small rocky exoplanet showing a transit depth of only a few hundred ppm [18]. The smallest exoplanet currently known to orbit a solar-like star is Kepler-37b [19] and it was discovered by the transit method. Its light curve along with the light curves of two other larger planets in the system are shown in Fig. 2.

2.3 Transmission spectroscopy and exo-atmospheres

Over the past decade, the characterization of exo-atmospheres has started to gain in importance. The first detection of sodium in the exo-atmosphere of a gas giant HD209458b was made from space with the Hubble Space Telescope (HST) [20],

Fig. 2 Figure shows a comparison of light curves obtained with *Kepler* for various sized exoplanets from the system Kepler-37, with the smallest being Kepler-37b (upper panel). Reprinted by permission from Springer Nature: Nature, [19] DOI: [10.1038/nature11914](https://doi.org/10.1038/nature11914), © 2013.



followed by the spectroscopic detection, also with HST, of an extended hydrogen atmosphere for the same planet [20, 21]. Ground based detection of exo-atmospheres with the transmission spectroscopy method using high spectral resolving power succeeded nearly six years later when sodium was detected in the atmosphere of HD 189733b [22].

Transmission spectroscopy uses the basic idea that, during a transit, the stellar light has to pass through the exo-planetary atmosphere which forms a thin annulus around the planet. If the atmosphere contains an absorber, such as sodium or any other species, the radius of the planet appears larger at the corresponding wavelength as the species blocks the stellar light.

When using transmission spectroscopy, typically, a time series of spectra with low spectral resolving power is recorded before, during, and after the transit. Each of the observed spectra from the time series is split into defined photometric bands and then the resulting spectrophotometric light curves are produced and evaluated. The variation in transit depth in the different spectral bands provides information on the absorbing species. This method has successfully confirmed atmospheres for a handful of planets. A metal rich atmosphere was confirmed for the Neptune-sized exoplanet GJ1214b from the ground [23, 24], followed by many other detections for predominantly gas planets [25, 26]. Lately, reports of elements other than sodium and hydrogen have been reported, such as lithium and perhaps a first detection of

TiO features [26, 27]. However, this method also has potential application to rocky planets around late type dwarfs [28] that are recently discovered by TESS and will be found later by PLATO and ELT from the ground.

A slightly different approach is to use a spectrograph with high resolving power. A spectroscopic time series is again obtained on either side of, and during, the transit. In this case the actual spectra from in- and out-of-transit phase are directly compared. Before a search for planetary atmosphere signatures can start, a careful analysis of the telluric features in the spectra has to be performed and, if necessary, telluric features are removed [29]. Furthermore the Rossiter-McLaughlin effect which can affect the planetary signal needs to be taken into account [30]. Regions of prominent lines, such as the sodium doublet (NaD), or potassium region as well as hydrogen lines are typically investigated. The ratio of in- and out-of-transit spectra can reveal a planetary signature [22, 31, 32, 33, 34, 35] as the in-transit spectra also possess an excess signal from the planetary atmosphere.

2.4 Observing strategies of exoplanetary space missions

The detection of exoplanets is most efficient from space with the transit method. Therefore, we will introduce the observing strategies and principles of such missions. Different space missions dedicated to the search of planets via transit detection have followed different observing strategies. The first one, CoRoT, monitored several fields for a series of long (150 days) and short (30 day) periods. On the contrary, the space mission *Kepler* monitored a single field for 4 years. The selected field in the region of the Cygnus and Lyra constellations contained more than 150,000 stars [7] that were monitored. This part of the *Kepler* mission yielded about 2000 exoplanets and several thousand candidates. In 2013 the *Kepler* team needed to adopt a different observing strategy due to problems with the spacecraft gyroscopes. The mission was renamed *K2* and it observed one field for typically 70 days and then pointed towards a new field. Over the ensuing four years, the *K2* mission yielded about 1000 exoplanets and several hundred additional candidates [36]. There were numerous interesting discoveries among these missions, and many “firsts” reported, such as: the circumbinary planet Kepler-16b [37], the oldest known multiplanet system Kepler-444 [38], the first *Kepler* rocky planet Kepler-10b [39], and the first planet with a radius smaller than the Earth [40]. The *K2* mission was retired in late 2018 when the fuel was depleted.

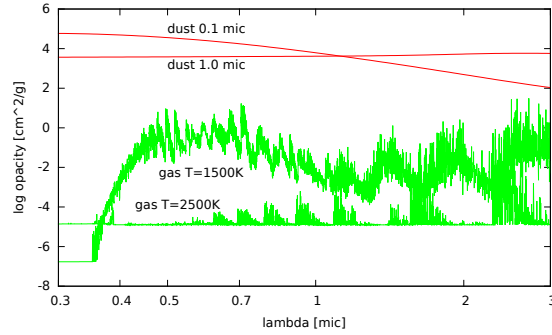
However, *Kepler* also discovered a new class of ‘disintegrating’ planets. In the following text, we lay the theoretical ground for understanding these highly enigmatic planets among the known types of exoplanetary systems.

3 Dust environment in exoplanets

In this section we introduce the basic physical properties of astrophysical dust which will be important for understanding the subsequent sections. At sufficiently low temperatures and high density, grains of condensates can be formed out of a gas phase. Such grains are usually called “dust”, although some authors use the more generic term “condensates”. At the same time, the term “grain” often includes not only solid grains but also liquid droplets. Such condensates are usually confined to “clouds”. These can not only be clouds in the atmospheres of cool objects but also vast interstellar dust clouds.

The reason why dust is so important for our objects will become obvious from the following everyday experience. Our atmosphere contains water. If this water is in the form of a gas one can easily see distant mountains which are 100 km away. However, once the water condenses and forms clouds or a fog, the visibility can drop to 10 meters or even less. Thus the opacity, which is a measure of the non-transparency of the material (see Sec.3.2), could be much higher if the material were in the form of dust rather than gas. Figure 3 illustrates the opacity of gas and dust in the visible and near infrared regions per gram of material. The opacity of the gas in this example is based on an assumed solar chemical composition and a density $\rho = 10^{-14} \text{ g cm}^{-3}$ [41]. For the dust opacity we used the illustrative mineral forsterite with a particle size of about 0.1 and 1 micron [42]. It should be mentioned that, as a rule, not all the gas can turn into a condensate. For solar composition material, dust can account for roughly 1% of the mass. Still, as can be seen from the figure, the dust opacity will easily overtake that of the gas.

Fig. 3 Comparison between the gas opacities at two temperatures and dust opacity of forsterite for two particle sizes.



3.1 Absorption, Scattering, and Extinction

The optical properties of condensates may not only influence, but fully govern, the emerging spectrum and even the structure of a dusty object. Dust can absorb the

impinging radiation and convert it directly into heating the grains. This process is called ‘absorption’ or ‘true absorption’ to emphasize that the photon is destroyed or thermalized. It is quantified by the absorption opacity.

Dust can also scatter the radiation in a process called ‘scattering’. Scattering mainly changes the direction of the photon without significantly affecting its energy. So the scattered radiation is somewhat decoupled from the medium and flows through and around it without heating it. This process is characterized by the scattering opacity. Furthermore, scattering can be highly anisotropic, a property that is described by means of the phase function, which depends on the scattering angle (the deflection angle from the original direction of the impinging radiation). The most prominent feature is a strong forward scattering peak for large values of the so-called ‘scaled particle size’, $X = 2\pi a/\lambda$ where a is the particle size (radius) and λ is the wavelength of the radiation.

The combined effect of absorption and scattering is referred to as the ‘extinction’. Finally, formation of dust can also affect the chemical composition of an object. It removes the condensed elements from the gas phase within the dust cloud. Subsequently, various processes and forces may decouple gas and dust, creating chemical inhomogeneities.

Absorption and scattering by large particles (relative to the wavelength, i.e., large X) is wavelength independent. However, *scattering* by small particles has a very strong, λ^{-4} , dependence (Rayleigh scattering) and *absorption* by small particles has a λ^{-1} dependence. Blue light is scattered and attenuated more efficiently, and for this reason dust generally causes a reddening of the light passing through a dust cloud. The extinction at some wavelength (or filter) in magnitudes is the difference between the observed and intrinsic brightness: $A(V) = V_{\text{obs}} - V_{\text{int}}$. Reddening (selective extinction/color excess) is usually expressed as a difference between the observed and intrinsic color index:

$$E(B - V) = (B - V)_{\text{obs}} - (B - V)_{\text{int}} = A(B) - A(V) \quad (3)$$

A relative slope of the wavelength dependence of the extinction can be characterized by a single parameter $1/R(V)$ where $R(V)$ is [43]:

$$R(V) = \frac{A(V)}{E(B - V)} = \frac{A(V)}{A(B) - A(V)} \quad (4)$$

$R(V)$ is sensitive to the particle size. The typical value of $R(V)$ for interstellar dust in our Galaxy is 3.1 ± 0.2 . The absolute amount of the extinction as a function of λ (the extinction curve) can be characterized by two parameters: $R(V)$ and $E(B - V)$.

3.2 Cross-section, Opacity, and Phase Function

The optical properties of the dust are given by the complex index of refraction of the material it is made from (which is a function of wavelength), and further depends on

the size and shape of the particles. These properties of the grains are often expressed in the form of cross-sections for absorption, scattering, and extinction C_a , C_s , C_e , respectively. The cross-sections are related to the projected area of the dust particles of radius r via efficiency factors Q_a , Q_s , and Q_e , for absorption, scattering, and extinction, respectively:

$$C_a = Q_a \pi r^2, \quad C_s = Q_s \pi r^2, \quad Q_e = Q_a + Q_s. \quad (5)$$

The cross-sections are related to the absorption and scattering opacities, $\kappa_{\nu,a}$ and $\kappa_{\nu,s}$, of the condensates at radiation frequency, ν , by:

$$\kappa_{\nu,\{a,s\}} \equiv C_{\nu,\{a,s\}}/m_g = \frac{3}{4} \frac{Q_{\nu,\{a,s\}}}{\rho_g r} \quad (6)$$

where κ is the cross section per unit mass and has the dimensions of $\text{cm}^2 \text{g}^{-1}$, m_g is the mass of a dust grain, ρ_g is the bulk material density of the grain, and we have assumed spherical particles for simplicity. Note that κ is nearly exclusively a property of the material and may not depend at all on the mass in dust grains per unit volume of the medium, $\bar{\rho}$. Finally, for completeness, we note that the quantity $\alpha \equiv \bar{\rho} \kappa$ is defined as the linear extinction coefficient (with units cm^{-1}), and may be useful in certain circumstances.

Using these opacities, the monochromatic optical depth due to scattering and absorption along the line of sight z is then given by:

$$\tau_\nu = \int \bar{\rho}(z) [\kappa_{\nu,a}(z) + \kappa_{\nu,s}(z)] dz. \quad (7)$$

The sum of the absorption and scattering opacities is referred to as a total opacity. For the special idealized case of single-size dust particles, this reduces to

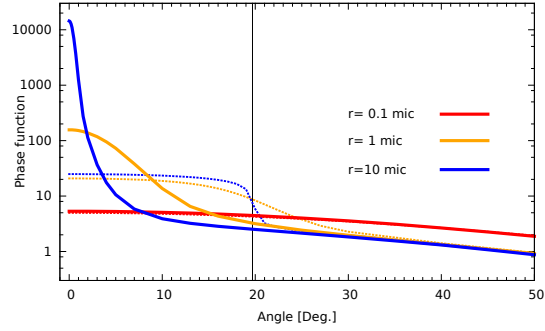
$$\tau_\nu = \frac{3}{4} \frac{(Q_{\nu,a} + Q_{\nu,s})}{\rho_g r} \int \bar{\rho}(z) dz. \quad (8)$$

We can see from this, that for a fixed amount of dust mass per unit volume of the medium, i.e., $\bar{\rho} = \text{constant}$, the optical depth would become monotonically larger with decreasing particle size, as $1/r$. However, in Mie scattering, once the particle size becomes substantially less than the radiation wavelength, $\lambda = c/\nu$, then the Q factors for the cross section drop dramatically, and the optical depth stops rising with further decreases in particle size. This is the reason why, for observing wavelengths in the visible, it is often stated that particle sizes comparable to a micron are the most efficient at blocking light.

The angular distribution of the scattered light is described by the phase function, $p(\theta)$, where θ is the scattering angle which measures the deflection of the scattered photon from its original direction. The phase function is normalized such that its integral over all solid angles is 4π . An example of the dust phase function at small angles is displayed in Figure 4. One can see a strong increase towards zero phase

angle which is called the forward scattering peak. The amplitude and width of this peak are quite sensitive to the particle size and wavelength. Calculations of phase functions usually assume an incident parallel beam of light. However, if the dust cloud were very close to the star, its angular dimension (as seen by the dust grain) could be comparable to, or wider than, the width of the forward scattering peak. This will be the case in our objects and one has to take that into account [44, 45, 46]. The same figure also illustrates this effect on dust particles located in the atmosphere of the exoplanet WASP-103b [47, 48].

Fig. 4 Phase functions assuming a point source of light (solid) versus the phase functions assuming the finite dimension of the stellar disc (dotted). Example is for enstatite at 600 nm for different dust particle radii. The vertical line illustrates the angular radius of the stellar disc of WASP-103 as seen from the planet WASP-103b.



It is sometimes useful to define a mean cosine of the scattering angle g , also known as the asymmetry parameter. It has values from -1 to 1 and is calculated from the phase function:

$$g = \int p(\theta) \cos(\theta) d\Omega / 4\pi. \quad (9)$$

3.3 Albedo, Equilibrium Temperature, and Radiative Acceleration

Let's assume that a dust particle is irradiated by its host star with effective temperature T_* , solid angle Ω_* , and intensity approximated by the Planck function $B_\nu(T_*)$. The particle can scatter some of the light from the star, and we define a quantity called single-scattering albedo, ϖ , which describes the reflecting properties of the grains. It is a fraction of the energy which is scattered by the particle:

$$\varpi_\nu = \frac{C_{\nu,s}}{C_{\nu,a} + C_{\nu,s}}. \quad (10)$$

This scattered light does not heat the particle. Apart from scattering, the particle can also absorb the stellar radiation at a rate:

$$\Omega_* \int C_{\nu,a} B_\nu(T_*) d\nu \quad (11)$$

This energy heats the particle to a temperature T_g . Subsequently, the grain emits thermal radiation and cools at a rate:

$$4\pi \int C_{\nu,a} B_{\nu}(T_g) d\nu, \quad (12)$$

A balance between the absorbed and re-radiated energy sets the grain equilibrium temperature (provided that the grain is not also sublimating; but see Eqn. 21). It can be obtained by solving the radiative equilibrium equation for T_g :

$$\Omega_* \int C_{\nu,a} B_{\nu}(T_*) d\nu = 4\pi \int C_{\nu,a} B_{\nu}(T_g) d\nu \quad (13)$$

Assuming that the opacities are grey (i.e., they do not depend of the frequency) the grain temperature is simple given by:

$$T_g^{\text{grey}} = T_* \left(\frac{\Omega_*}{4\pi} \right)^{1/4}. \quad (14)$$

A dust grain irradiated by a star with effective temperature T_* , mass M_* , radius R_* , and surface flux F_* , experiences a radiative acceleration a_R . It is usually expressed as a parameter β relative to the gravitational acceleration a_G :

$$\beta = \frac{a_R}{a_G} = \frac{R_*^2}{GM_*c} \int [\kappa_{\nu,a} + (1 - g)\kappa_{\nu,s}] F_{\nu}(T_*) d\nu. \quad (15)$$

where G is gravitational constant, c is speed of light, and g is the previously mentioned asymmetry parameter. Thus, in the two extreme cases of forward vs back scattering of the stellar radiation, the scattering adds either nothing to the radiative acceleration or has a factor of 2 enhancement relative to the absorption term.

Extensive online tables of such dust properties devoted mainly to exoplanets are publicly available [42]. They are based on codes that calculate cross-sections of dust particles using Mie theory such as [49] from the complex indices of refraction for specific materials. For example, the Heidelberg - Jena - St.Petersburg - Database of Optical Constants is a very convenient source of refractive index measurements [50, 51].

3.4 Dust Condensation

Depending on the state quantities, such as temperature and pressure, matter composed of a single component usually exists in one particular phase, e.g. gas, liquid, or solid. The Clausius-Clapeyron equation, which gives a relation between the temperature and pressure, marks a transition or boundaries between the different phases. Once the temperature drops below the condensation temperature (at a certain pressure) or the pressure exceeds the equilibrium (saturated) vapour pressure (at a particular

temperature) the dust starts to condense out of the gas. Condensates may be in either the liquid or solid phase. The equilibrium vapor pressure where the transition occurs can be approximated by [52, 53]:

$$P_v(T) = \exp(-A/T + B) \quad (16)$$

where A, B are material-specific sublimation parameters.

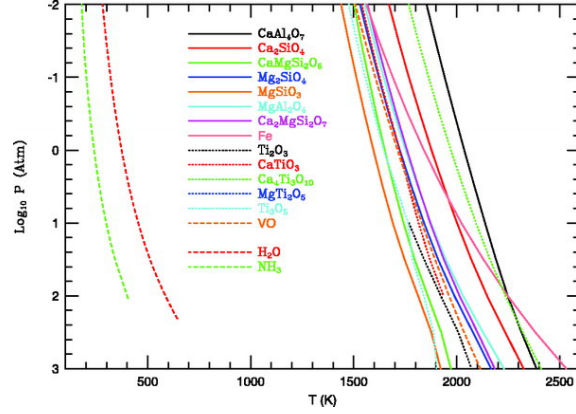
Materials with low vapour pressure or high condensation temperature (refractory materials) condense first out of a hot cooling gas (or last to evaporate if the dust were heated). For a solar chemical composition these are mainly calcium and aluminum oxides such as corundum (Al_2O_3), grossite (CaAl_4O_7) and hibonite ($\text{CaAl}_{12}\text{O}_{19}$). They are followed by titanium compounds such as perovskite (CaTiO_3) or TiO_2 at lower temperatures. The most important refractory species are usually silicates. They form two branches: pyroxenes ($\text{Mg}_x\text{Fe}_{1-x}\text{SiO}_3$) and olivines ($\text{Mg}_{2y}\text{Fe}_{2-2y}\text{SiO}_4$). In each branch a fraction of magnesium atoms can be replaced by iron. Iron free pyroxene is called enstatite (MgSiO_3) while an iron free olivine is forsterite (Mg_2SiO_4). The other extreme member of the olivine family is fayalite (Fe_2SiO_4). Silicates are a type of glass and, as such, are quite transparent in the optical region, although they can scatter light quite efficiently. The amount of iron can affect their absorption properties significantly [54]. Other refractory dust species which might be encountered in such an environment are amorphous carbon, graphite (C), silicon carbide (SiC), Quartz (SiO_2), spinel (MgAl_2O_4), or akermanite ($\text{Ca}_2\text{MgSi}_2\text{O}_7$). At the other end of the condensation temperature scale are volatile species such as water and ammonia. In between are numerous compounds, depending on the chemical composition and pressure, for example sulfides and alkali halides, and troilite but we are not likely to observe these in such hot and close disintegrating objects.

Apart from the temperature, the occurrence of a particular dust component also depends critically on the abundances and the availability of the chemical elements which form the compound. The element with the lowest abundance is typically the limiting factor for the abundance of the whole compound. The solar abundances² of Ca, Al, and Ti are relatively small 6.34, 6.45, and 4.95, respectively [55]. That is why silicates and/or iron dust which are composed of silicon, magnesium, and iron with abundances of 7.51, 7.60, and 7.50, respectively are usually more abundant and dominate extinction processes.

The condensation properties of various compounds are nicely summarized in Figure 5. Here the condensation curves are plotted as a function of atmospheric pressure. They were calculated mainly for the atmospheres of brown dwarfs or giant exoplanets and assume a solar chemical composition [56] but contain many dust species which are also relevant for our objects.

² Note that the abundances are defined, using the element number density N , as the number of atoms of an element per 10^{12} atoms of hydrogen ($\log N/H + 12$). The present-day solar photospheric abundances are generally in a good agreement with the abundances derived from the CI carbonaceous chondrite meteorites, except for a few elements such as H, He, and Li.

Fig. 5 Condensation temperatures of several compounds as a function of atmospheric pressure assuming a solar composition gas. Taken from [56]. Courtesy of ApJ.



3.5 Dust Sublimation

Dust particles are also subject to sublimation [52, 53]. The mass-loss flux (rate per unit area) from a solid surfaces at temperature T in vacuum is

$$J(T) = \alpha P_v(T) \sqrt{\frac{\mu u}{2\pi k_B T}}, \quad (17)$$

where α is the evaporation coefficient, $P_v(T)$ the equilibrium vapor pressure, μ the molecular weight, u the atomic mass unit, and k_B Boltzmann's constant. The mass-loss rate from a spherical dust grain of mass $m_g = 4\pi r^3 \rho_g / 3$ and surface area $S = 4\pi r^2$ is then

$$\frac{dm_g}{dt} = -SJ. \quad (18)$$

Taking into account that

$$\frac{dm_g}{dr} = S\rho_g \quad (19)$$

the change in the particle radius is given by:

$$\frac{dr}{dt} = \frac{dr}{dm_g} \frac{dm_g}{dt} = -\frac{J}{\rho_g}. \quad (20)$$

Sublimation represents a phase transition which consumes heat and cools the particle. If that heat is not negligible one has to take it into account in computing the equilibrium temperature of the grain. In such a case the energy absorbed by the particle per unit time is balanced by the energy radiated by the particle plus the heat consumed for the phase transition. Equation 13 then reads

$$\Omega_* \int C_{v,a} B_\nu(T_*) d\nu = 4\pi \int C_{v,a} B_\nu(T) d\nu - \mathcal{L} \frac{dm_g}{dt} \quad (21)$$

where \mathcal{L} is the latent heat of sublimation per unit mass. The characteristic timescale for sublimation is

$$\tau = \frac{m_g}{|dm_g/dt|}. \quad (22)$$

4 Known Disintegrating Exoplanets

The great majority of exoplanets that we know of were discovered by the transit method. Nominal planet transits are symmetric and periodic without any significant variations in their shape or depth over time. This changed in 2012 when a strange object named Kepler-1520-b was discovered [57].

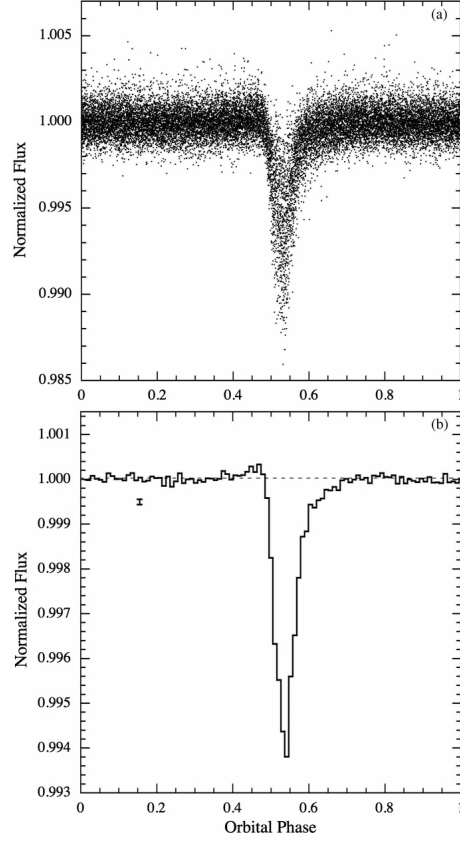
4.1 Kepler-1520b

Kepler-1520b is an exoplanet also known as KIC 12557548b (KIC1255b). It became a prototype of a very rare new class of exoplanets called Disintegrating Exoplanets. It was found in the *Kepler* data. The host star is a V=16 mag main sequence K4V type star. Its effective temperature, mass, and radius are about $T_{\text{eff}} = 4440$ K, $M = 0.7M_{\odot}$, and $R = 0.65R_{\odot}$, respectively [57, 58]. The star is active and has spots which cause $\sim 1\%$ variability with a period of about 22.9 days which enabled its rotation period to be determined [44, 59]. In its light curve, the discoverers noticed something like transits but they were highly variable, sometimes as deep as 1.2%, sometimes even missing. The strictly periodic transit signal had a very short period of about 15.7 hours. Figure 6 illustrates the observed data folded with this period which yields the average light curve. One can see a significantly increased spread of fluxes in the points during the transit indicating the variability in the transit depth. Another interesting feature becomes obvious from the binned and averaged light curve (bottom panel of Fig. 6). It is highly asymmetric and features a steeper ingress and slower egress. The strict periodicity and short period of the transits indicate that they may be caused by some body orbiting the star on a very close orbit. The fact that the transits are sometimes missing implies that the body itself is very small, smaller than the Earth, otherwise it would be detected in every transit. Follow-up radial velocity measurements did not detect any reflex motion of the star which puts an upper limit on the mass of the body of $89 M_{\oplus}$ [60, 61] which places the body deep into the planetary regime. However, what is then causing the variable asymmetric transits?

4.1.1 Interpretation

The interpretation is that a body on such tight orbit around the star is heated to about 2000 Kelvin. At such temperatures even rock melts and can evaporate which may drive a thermal wind off the surface [57, 62]. Gas escapes the planet at a rate larger

Fig. 6 Top: First long cadence Kepler observations of KIC 1255 folded with the 15.7-hr orbital period. Bottom: Binned and averaged light curve. Taken from [57]. Courtesy of ApJ.



than $0.1 M_{\oplus}/\text{Gyr}$ dragging dust grains with it. Alternatively, the dust may condense out of the gas when it cools during or after escape from the planet. The mixture of gas and dust expands beyond the Hill sphere radius of the planet. It flows “down hill” out of the potential well of the planet through the L1 point towards the star or via the L2 point away from the star. Strong radiative forces on the dust cause a weakening of the effective gravity which drives the dust into higher orbits that lag progressively behind the planet. It is this dust which is causing the transits and this is also the reason why we observe a steep ingress followed by a gradual egress.

Once such a fine dust cloud forms around and behind the planet it may not be stable and is prone to variability. For example when the dust cloud is thin the planet surface is intensively irradiated, which leads to more evaporation, outflows, and condensation, thereby producing more dust. In turn, the thick dust cloud shields the planet and the evaporation drops, limiting the production of dust, and the cloud dissipates. This limit cycle can apparently operate, even on a timescale from orbit to orbit, but there are longer intervals of order a week where the transits are reduced to a level where they are not detected (see also the following section on the variability).

Producing and maintaining a substantial outflow of gas and dust is relatively simple in bodies with the surface gravities of asteroids, where the thermal speed of the material exceeds the escape speed (see, e.g., Fig. 8 of [13]). For at least some common minerals the vapour pressure at ~ 2000 K is sufficiently high that for bodies below lunar size, the direct Jeans' escape mass loss rates could exceed that required to produce the inferred dust rates in KIC 1255b of $\sim 1 M_{\oplus}/\text{Gyr}$. For more substantial bodies, e.g., Mercury, Mars, and Earth, a Jeans' outflow of $1 M_{\oplus}$ per Gyr of heavy molecules becomes nearly impossible [57, 62, 13]. For such massive bodies, a different escape mechanism has been proposed, namely a Parker-type hydrodynamic wind [57, 62]. Roughly speaking this requires thermal speeds that are only $\sim 1/4$ of the escape speed in order to work [57, 62]. One issue with the requirement of a planet losing $1 M_{\oplus}$ per Gyr is that if it has of only $\sim 10^{-3} - 10^{-2} M_{\oplus}$, then it will have a lifetime of only 1-10 Myr. If the lifetime of the host star is measured in Gyr, then the a priori probability of seeing one of its planets in that evaporative state are rather low. However, obviously if one surveys a large number of stars, then the odds of seeing a few such systems is non-negligible. Since such planets may have lost most of their mass their observations open a unique window into planetary interiors and their chemical composition [63, 64].

4.1.2 Variability

It was mentioned above that the transits are variable. They vary on a very short timescale from one orbit to another, i.e., in less than one day. This variability is strong, sometimes more than a factor of 2 from one orbit to the next one, and appears to be stochastic and associated with the deep core of the transit [57, 65]. However, a modulation of the transit depth was also found that appears to be anti-correlated with the periodic rotational variability (22.9 days) of the stellar flux [59, 66].

There is also a smooth long-term variability in the egress part of the light curve associated with the dust tail on timescales of about 1.3 yr which is not seen in the core of the transit [44, 58]. There might also have been a period of decreased activity, i.e., when the transits were shallower on average, during 2013-2014 [67]. This longer-term variability in the depth and shape of the transits indicates that the dust cloud associated with the planet may not be homogeneous and has at least two components; an inner tail (or coma) and an outer tail which may behave differently (e.g., when subjected to magnetic fields or stellar winds) or have different properties (particle size, chemical composition) [44, 65]. On the contrary, [68] arrived at the conclusion that, as far as the pure shape of the average transit profile is concerned, it is well reproduced in their calculations and there is no need to invoke two such constituents. A similar long-term variability of the transit, namely a monotonic decrease of its depth over the four-year duration of the *Kepler* mission was found in another disintegrating exoplanet, KOI 2700b [69].

The reason for the above mentioned long-term variability has not been well studied but it has been argued that it may be associated with the magnetic activity of the star and be analogous to the comet tail disconnection events observed in some of

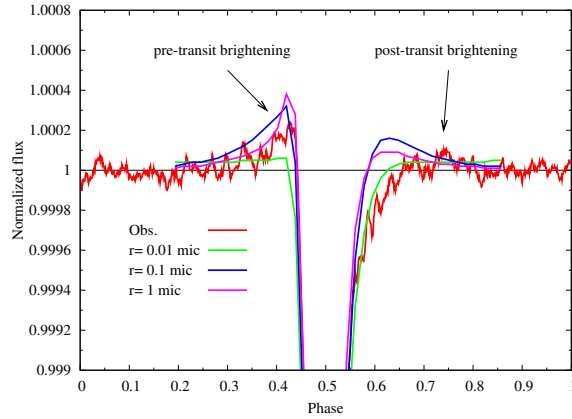
the comets in our Solar System [44, 59]. However, it has also been argued that the modulation of the transit depth with stellar rotation may be due to occultations of the stellar spots rather than the magnetic activity [66].

4.1.3 Pre-transit brightening

There is a very interesting tiny feature in the transit light curve, barely visible in Figure 6. It is a small brightening just before the transit, already noted by the discoverers [57], which is referred to as a pre-transit brightening. It is not due to the star getting brighter. It is caused by the scattering properties of the dust. As shown in Figure 4, the dust does not scatter the light isotropically but mainly in the forward direction. For the same reason a driver gets blinded when the Sun is near, but not in, the driver's immediate field of view, but the windshield is dirty and this nonetheless scatters the sunlight into his/her eyes.

In our system, this happens mainly in the vicinity of the transit. While we cannot identify this light during or after the transit, since it is overlaid with the ongoing absorption, we can see it just before the transit (Figure 7). This feature is sensitive to the particle size and it enables us to estimate that the size of particles in the tail is about 0.1-1 micron. At the same time this effect confirms that the transit events are caused by a dusty tail passing in front of, and close to, the star. Apart from these features in direct transits, the forward scattering effect can, in principle, be used to detect non-transiting dusty-tailed exoplanets by searching for positive bumps in the light curves [45, 46].

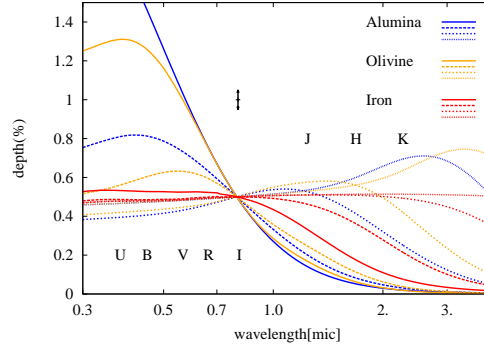
Fig. 7 *Kepler* light curve of KIC 1255 (red) zoomed so that the pre-transit brightening is clearly visible. Models (green, blue, purple) demonstrate that this feature is sensitive to the particle size. Taken from [44] and reproduced with permission ©ESO.



4.1.4 Particle size and chemical composition

A number of authors have studied the *Kepler* light curves of KIC 1255b attempting to derive the chemical composition and grain size distribution of the transiting dust material [70, 44, 65]. This problem is partially degenerate and one can fit such monochromatic³ transits with different chemical composition and particle size. The pre-transit brightening is sensitive to the particle size and the observed brightening indicates particles 0.1-1 micron in size. On the other hand, the length of the tail is highly sensitive to the sublimation properties of the grains. Corundum and 0.2-5 micron grains are most favoured for this reason and the mass loss rate amounts to 0.6-16 Earth masses per Gyr [53, 68].

Fig. 8 Theoretical transit depths for three species alumina, olivine, and iron; each for the particle size of 0.1 (solid), 0.16 (dashed), 0.4 (short-dashed), 1.0 (dotted) micron as a function of wavelength. Depth is normalized such that the transit in the I filter is about 0.5% deep.



More information and a deeper insight can be achieved with multi-wavelength observations. This is because the opacity of dust changes with the wavelength and the behaviour is different for grains of different chemical composition and size. Consequently, under the assumption that the tail is optically thin, the transit depth would depend on the wavelength, the particle size, and the chemical composition. This is illustrated in Figure 8 which shows theoretical transit depths for three species: corundum (alumina), olivine, and iron. One can see that the transits produced by small particles of corundum or silicates would be much deeper at the shorter wavelengths. This is because scattering dominates extinction and scattering on small particles (relative to the wavelength) is approaching the Rayleigh regime with a strong λ^{-4} dependence. Extinction by large particles is almost grey. The problem is that the observations must be carried out at different wavelengths simultaneously because of the above mentioned strong variability of the transit depths.

Such observations in the optical and near-infrared regions have not detected a significant difference in the transit depth across these wavelengths. This implies that the dust particle size must be larger than ~ 0.5 micron. In a scenario where

³ In this context ‘monochromatic’ means transits that are observed in only a single waveband.

dust grains are lifted directly from the surface of the planet, this in turn implies that the planet should be less massive than Mercury otherwise its gravity would prevent such direct dust ejection [60, 67]. However, as mentioned above, dust might have also condensed later beyond the potential well of the planet. Additional multi-wavelength observations in z' , g' , u' filters indicate slightly larger depths at shorter wavelengths and particle sizes of about 0.25-1 micron [71]. Recent 3D models of the dust dynamics including the sublimation and 3D radiative transfer pointed out the possibility that the tail may be optically thick. In this case the transit depth might be constant with the wavelength even for smaller particles and mass loss rates may reach 80 Earth masses per Gyr [64].

Apart from KIC 1255b, two other systems of this kind have been discovered, KOI 2700b [69] and K2-22b [72]. The first one is similar in its transit profile to KIC1255b, and the latter system is described in more detail below.

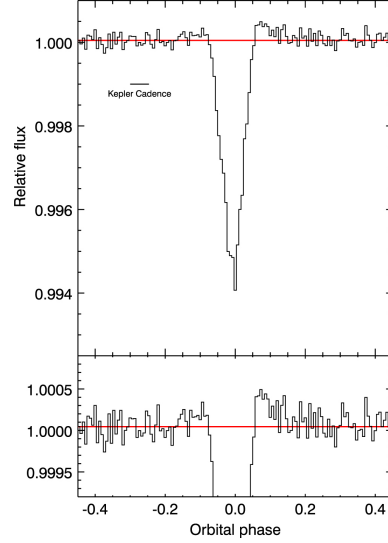
4.2 K2-22b

This exoplanet (also known as EPIC201637175B) was discovered with the *Kepler* follow-on mission (K2) by [72]. It is in some respects similar to KIC 1255b. The host star is cooler and smaller. It is an M0V type red dwarf ($r = 15.01$ mag) with effective temperature, mass, and radius of about $T_{\text{eff}} = 3830$ K, $M = 0.6 M_{\odot}$, and $R = 0.57 R_{\odot}$, respectively. The host star rotates with a period of 15.3 days and has a ‘close’ (3 magnitudes fainter) companion, separated by about $2''$. The planet K2-22b is smaller than $2.5 R_{\oplus}$, is less massive than $1.4 M_J$, and has a very short orbital period of only 9.145872 ± 0.000024 hours. It is losing mass in the form of a dusty tail at a rate $\approx 2 \times 10^{11} \text{ g s}^{-1}$ [72].

As in the case of KIC 1255b, the transits are asymmetric and highly variable. They are on average about 0.5% deep but the depth changes from 0 to 1.3% from transit to transit. The duration of the transits is about 50 minutes. The average transit shape is shown in Figure 9. The special feature of this exoplanet is that it exhibits a post-transit brightening. Based on the lesson learned from KIC 1255b, this likely indicates that the planet also has a dusty tail but it is pointing in the opposite direction. In other words, the planet is orbiting the star with its dust tail heading forward. This is most probably due to the host star being colder and fainter than KIC 1255. Its radiation does not exert sufficient pressure on the dust grains to force them into a higher orbit, and thereby trail the star. Thus, the dust can flow from the planet toward the L1 point and the host star, and then descend into the potential well of the star. Since the Keplerian velocity of these orbits is higher, these grains overtake the planet and form a leading dust tail [72].

The follow up multi-wavelength transit observations with the GTC in the visible region found no evidence for a wavelength dependence in three out of the four transits observed [72, 73]. One transit, however, did indicate that the transit depth is greater at the bluer wavelengths. This sets an upper limit on the dust grains of about 0.4-0.6 micron. The forward scattering peak indicates particle sizes of about 0.5 micron.

Fig. 9 Binned and averaged *K2* light curve of K2-22 folded with the orbital period. It features a post-transit brightening likely indicative of a leading dust tail. Taken from [72]. Courtesy of ApJ.



Although the dust is the major opacity source, the gas might be detected in the cores of some strong spectral lines such as NaI in high resolution spectra. [74] searched for such gas absorption during the transits of K2-22b and Kepler-1520b but did not detect any spectral signatures.

5 Minor bodies in Extrasolar systems

As in our solar system, minor bodies are also expected to exist in extrasolar systems. While we do not yet have the capability to detect structures similar to the main asteroid belt or the Oort cloud in other planetary systems, the first extrasolar minor bodies have recently been detected.

5.1 Exo-Asteroids: a debris disk around WD 1145+017

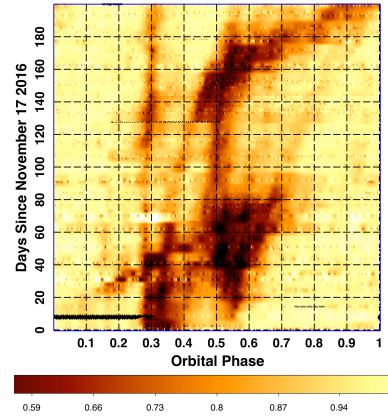
In the solar system, asteroids are defined as minor bodies in the inner solar system that show significant departures from spherical shape dictated by hydrostatic equilibrium. The first extrasolar minor bodies were discovered by *K2* [75] in the form of disintegrating material orbiting the white dwarf WD 1145+017.

It has long been known that some white dwarfs have dusty debris disks around them [76, 77], and also that many of them (about 1/4 - 1/2) have heavy elements in their atmospheres that should have already sunk into the stellar interiors, unless they were replenished by infalling orbiting material [78, 79, 80]. Vanderburg et al

[75] observed for the first time this process in action by detecting a white dwarf being transited by ‘at least one and likely multiple disintegrating planetesimals with periods ranging from 4.5 hours to 4.9 hours’. The detected transits are marked by being asymmetric, and even irregular, with respect to normal transiting planets, indicating that they do not correspond to solid spherical bodies, and can be as deep at 55 per cent. In addition, most of the observed transits are much longer in duration than the ~ 1 -2 min expected transit time of an asteroid with an orbital period of 4.5 hour. Note that the white dwarf radius and luminosity are quite low. Its apparent brightness, luminosity, distance, effective temperature, mass, and radius are about $g = 17.0$ mag, $L = 0.0093 L_{\odot}$, $d = 174$ pc, $T_{\text{eff}} = 15900$ K, $M = 0.6 M_{\odot}$, and $R = 1.4 R_{\oplus}$, respectively. The orbital period of 4.5h corresponds to a distance of about $1 R_{\odot}$ from the star. A combination of this distance and stellar luminosity yields equilibrium temperatures of about 1400-1700 K which is similar to those of disintegrating planets.

This object has attracted the attention of exoplanet observers. Croll et al. [81] conducted ground and space follow-up observations on WD 1145+017. The observations confirmed that the white dwarf is orbited by multiple short-period objects, that egress times were longer than ingress times, and the duration of the transits was longer than expected, pointing again to cometary tail-like structures behind the debris fragments. These asteroids are nicely visualized with a ‘waterfall’ diagram presented in Rappaport et al. [82] showing the evolution of the phase light curve (see Fig.10). One can easily identify several objects with slightly different periods crisscrossing the picture.

Fig. 10 Waterfall diagram of WD1145 phased with the base period of 4.49126 days. Objects with the base period follow the vertical line while objects with different periods crisscross the diagram on different tracks. Taken from [82] by permission of Oxford University Press.



Croll et al. [81] also did not detect any transit chromaticity. Alonso et al [83] and Izquierdo et al [84] used the 10-m GTC telescope to check for chromaticity but found the transits to be gray over the optical range from 480 to 920 nm (see Figure 11), indicating that particle sizes smaller than 0.5 micron can be excluded. From their observations, Alonso et al [83] concluded that the radius of single-size particles in the tail materials must be $\approx 0.15 \mu\text{m}$ or larger, or $\approx 0.06 \mu\text{m}$ or smaller. They also

report low amplitude variations in the light curves suggesting that dusty material is continuously passing in front of the stellar disk.

Zhou et al. [85] and Xu et al [86] also observed these dips in multiple photometric bands in the visible and infrared. They find no difference in the transit depths once infrared observations are corrected for excess emission from a dusty disk. Xu et al [86] conclude that there must be a deficit of small particles in the transiting material and that only large particles can survive without sublimating at the effective temperatures prevalent at these short orbital periods.

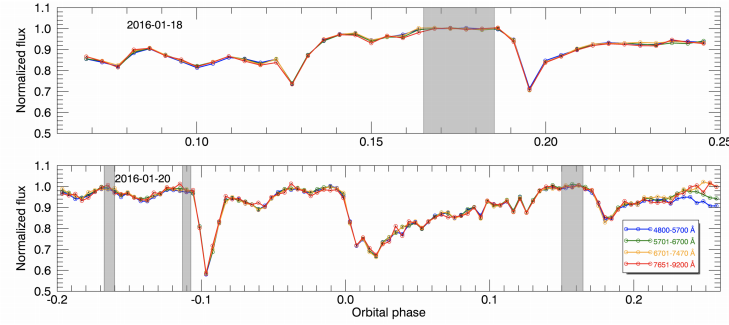


Fig. 11 GTC light curves of WD 1145+017 taken simultaneously in four wavebands and covering several dips. The nearly identical dip profiles in the four bands can be used to constrain the dust grain sizes to larger than $0.5 \mu\text{m}$. The divergence of the curves after phase 0.22 in the lower panel is due to atmospheric effects. Adapted from [83] and reproduced with permission ©ESO.

Xu et al. [87] found the first detection of chromaticity, showing that UV transit depths are always shallower than those in the optical. They proposed a model to explain this observations by having the transiting dust clouds block a larger fraction of the circumstellar gas than of the white dwarf and by having all of them (transiting dust, circumstellar gas, and white dwarf) aligned with respect to our line of sight.

The light curve of this object is extremely variable as shown by Rappaport et al. [88, 82] and Gänsicke et al. [89]. This is because (i) individual objects have slightly different periods, (ii) the periods of some of individual objects can change slowly with time, and (iii) their dust activity can change dramatically on timescales of months and years.

High resolution spectroscopic observations also revealed the presence of high-velocity gas orbiting the white dwarf. [90, 91].

A more detailed review of this object can be found in [82, 92]. Very recently a second white dwarf with possibly related properties was discovered [93]. This object, ZTF J013906.17+524536.89, exhibits two deep transits separated by 110 days, but it is not yet clear if this is a periodicity.

5.2 Exo-comets

The unprecedented precision of the *Kepler* photometry enabled the detection of even smaller objects than planets or even large asteroids. Two decades ago [94] predicted that comets orbiting other stars and emitting large dusty tails might be detected by photometry when transiting their host stars and calculated what their light curves could look like. In the *Kepler* data, [95] detected six events in the light curve of KIC 3542116 (KIC3542) and one event in the light curve of KIC 11084727 (KIC1108) which looked very much like the expected cometary transits. They were about 0.05-0.2% deep and highly asymmetric, similar in shape to the KIC1255b transits but several times more shallow (see Fig.12). The three deeper transits of KIC3542 and that of KIC1108 lasted for about one day while the three shallower transits of KIC3542 lasted for about half a day. There is no obvious periodicity to these events indicating that six transits of KIC3542 are caused by 2-6 distinct comet-like bodies. The duration of the transits corresponds to a transverse speeds of about 35-50 km/s for the longer transits and about 75-90 km/s for the shorter transits. This corresponds to orbital periods of ≥ 90 and ≥ 50 days, respectively. Both host stars KIC3542 and KIC1108 are relatively bright ($V=10$ mag) and hot stars

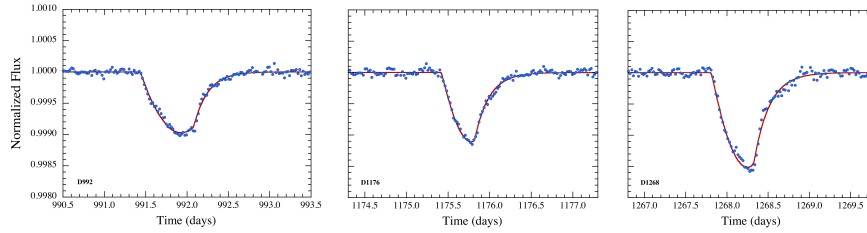


Fig. 12 Three deeper transit events found in the Kepler light curve of KIC3542 by [95] by permission of Oxford University Press.

with $T_{\text{eff}} = 6900$ and 6800K , respectively. Most of the stars monitored by *Kepler* are cooler (or older) so the fact that they are hotter/younger, similar to each other, and also similar to Boyajian's star mentioned later is probably not an accident.

Recently, a single comet-like transit was found in the archival lightcurve of KIC 8027456 [96]. The *TESS* mission also detected three other dips of this kind in β Pictoris [97]. Similar events were discovered in two stars (EPIC 205718330 and EPIC 235240266) monitored by the *K2* mission [98]. The authors call these 'little dippers' since they resemble the so-called "dipper" stars. However, contrary to dipper stars, these dips are 1-2 orders of magnitude shallower with depths of about 0.1-1%. The dips in the 'little dippers' are episodic, not periodic, lasting for about 0.5-1 days, with complicated shapes resembling more WD1145 or Boyajian's star rather than the typical exocomet like profile seen in Fig.12. Nevertheless, the authors argue that exocomets are the most likely explanation. The host stars are early-K and late-F type dwarfs, not younger than 150 and 800 Myr, respectively.

Recently, two other 'dipper' stars were discovered by K2 mission. HD139139 is a normal early G-type star which shows a sequence of 28 transit like dips [99]. The events are about 200 ppm deep, 0.7-7 hours long, are random, and do not show a significant asymmetry. EPIC204376071 is a young M5 dwarf which shows a single 80% deep asymmetric dip [100]. There is no explanation to these phenomena yet.

6 Boyajian's star

We would like to introduce another star which may be related to the above mentioned objects and which is sometimes labeled as "the most mysterious star in the Galaxy".

6.1 Discovery and the Kepler light curve

The *Kepler* mission delivered a huge amount of high-precision photometric light curves for about 170,000 stars. A group of volunteers, the 'Planet Hunters', were reviewing the light curves by human eye and they were the first to notice that there were some very strange dips in flux from the star KIC 8462852. A more detailed analysis and follow-up observations resulted in a discovery paper led by Tabetha Boyajian [11], and since that time the star has become known as Boyajian's or Tabby's star.

So what is so special about this star? The *Kepler* light curve shows a few strong dimming events that are 10%-20% deep. They are irregular with no sign of periodicity and are clustered into four main events observed near BKJD=790, 1520, 1540, 1570 days⁴. They are shown in Figure 13. The D790 event is very smooth with a slow ingress followed by a faster egress. The D1520 and D1570 events consist of a sequence of dips gradually increasing in strength. D1540 is a symmetric triple dip with the central dip being the strongest.

There is another tiny feature in the Kepler data at D1210 which deserves attention. It is a symmetric triple dip with the middle one being the strongest [101]. This shape resembles the D1540 event.

This kind of variability would not be anything unusual if this were a young star. Such stars are often surrounded by protostellar disks which might cause dipping events when seen nearly edge on. They show broad emission lines and infrared excess. However, this star has no such features and looks like a normal F3V type main sequence star with temperature, mass, radius, projected equatorial velocity and rotational period of $T_{\text{eff}} = 6750$ K, $M = 1.43M_{\odot}$, $R = 1.53R_{\odot}$, $v \sin i = 78$ km/s, and $P_{\text{rot}} = 0.88$ days, respectively [11, 102].⁵ It is a relatively bright, $V = 11.7$ mag star at the distance of about 451 pc. The authors also discovered a faint M dwarf

⁴ BKJD stands for the Kepler Barycentric Julian day which is a Julian Day minus 2454833

⁵ According to [103] the 0.88 day periodicity may come from a different source, not from the target star.

companion to the star at $1.95''$ which is about 3.8 mag fainter in H band. However, this star is not physically bound to Boyajian's star [104].

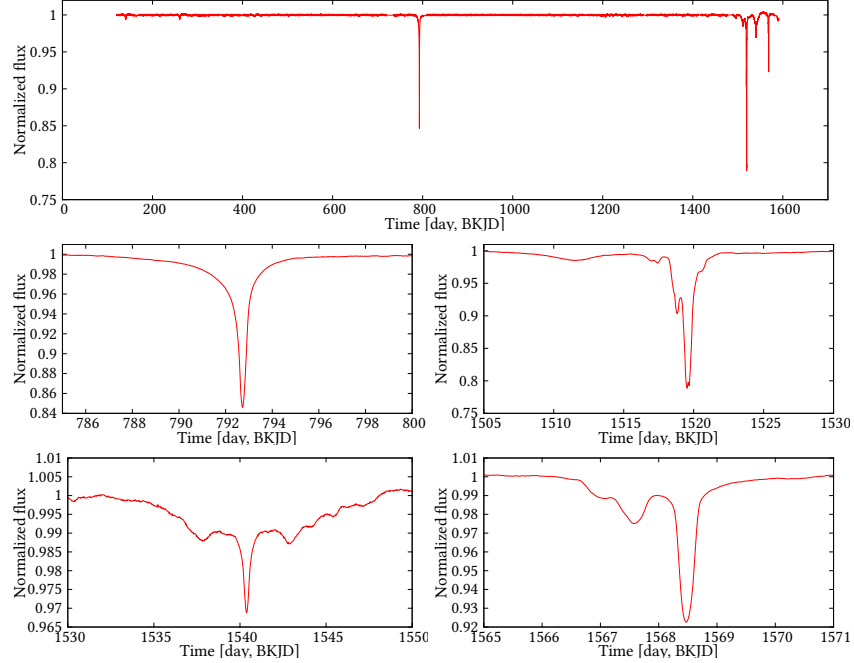


Fig. 13 The *Kepler* light curve of Boyajian's star shows irregular dips (top). A more detailed view of the four major events is displayed in the middle and bottom panels.

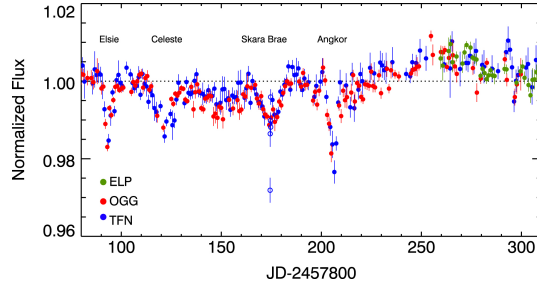
6.2 Follow up observations

Soon after the discovery of Boyajian's star, a plethora of follow-up observations were performed. Observations in the infrared region did not detect any infrared excess but put constraints on the amount of dust at different distances from the star. Spitzer/IRAC [105], NASA/IRTF 3 m SpeX [106], Millimetre (Submillimeter Array) and submillimetre (SCUBA-2) continuum observations also did not detect any significant emission towards KIC 8462852. This places an upper limit of about $10^{-6} M_{\oplus}$ of dust lying within 2-8 AU from the star, $10^{-3} M_{\oplus}$ located within 26 AU, and a total overall dust budget of $<7.7 M_{\oplus}$ within a radius of 200 AU [107].

Since the end of the *Kepler* space mission in 2013 May the star had been relatively quiet. In 2017 May the dipping activity started again with four main events named 'Elsie', 'Celeste', 'Skara Brae', and 'Angkor' shown in Figure 14 [108]. These dips are about 1%-2.5% deep. The multiband photometry of the dips shows differential

reddening favoring non-gray extinction. The data are inconsistent with dip models that invoke optically thick material, but rather they are in-line with predictions for an occulter consisting primarily of ordinary dust, where much of the material must be optically thin with particle sizes $\lesssim 1 \mu\text{m}$. No changes in the spectrum or polarization were detected during these events [108, 109, 110, 102]. Spectrophotometric observations of these recent dipping events with the GTC confirm that the dips are deeper in the visual than at red wavelengths. This is compatible with optically thin dust particles having sizes of $\approx 0.0015 - 0.15 \mu\text{m}$. Such particles would be quickly blown away by the radiation pressure which indicates that the dust particles must be continuously replenished [111]. Finally, we note that the radial velocities of the host star also seem to be constant, within 2 sigma from the average value of $v_{\text{rad}} = 4.21 \pm 0.02 \text{ km/s}$ [102]. This sets significant constraints on any companion stars or even brown dwarfs in short orbital periods.

Fig. 14 Boyajian’s star became active again in May 2017. Ground based monitoring shows four dips of depth 1-2.%. Taken from [108], courtesy of ApJ.



6.3 The long term variability

There is evidence for a long term (secular) variability of Boyajian’s star. Based on archival photographic plates from Harvard College Observatory, [112] found that the star faded at an average rate of 0.164 ± 0.013 magnitudes per century from 1890 to 1989. This result was questioned by [113, 114]. Nevertheless, a similar study using archival photographic plates taken at the Maria Mitchell observatory during 1922-1991 found a similar trend of 0.12 ± 0.02 per century [115].

The star’s brightness dropped significantly throughout the *Kepler* mission as well. Over the first 1000 days the star faded approximately by 0.9%. It dimmed much more rapidly in the next 200 days, with its flux dropping by more than 2% [116]. A slightly deeper 3.5% drop was found in the contemporary GALEX observation in the near UV [117]. These results imply $R_V \approx 5.0$ which, in turn, indicates circumstellar rather than interstellar dust attenuation.

Follow-up observations over a wide wavelength range from the UV to the mid-infrared from 2015 October through 2016 December, using Swift, Spitzer and AstroLAB IRIS indicate that the star faded in a manner similar to the long-term fading

seen previously in *Kepler* data. According to [118] the dimming rate for the entire period reported is " 22.1 ± 9.7 mmag per yr in the Swift wavebands, 21.0 ± 4.5 mmag in the ground-based B measurements, 14.0 ± 4.5 mmag in V, 13.0 ± 4.5 mmag in R, and 5.0 ± 1.2 mmag per yr averaged over the two warm Spitzer bands". Continued ground based observations [119, 120] suggest that there are also brightening (not only fading) spells and that this long term variability may be periodic with a period of 1600 days [119]. On the contrary, based on the ground and space based photometry spanning the 2006-2017 interval, it was concluded [121] that if the long term trend were to be periodic then the period would have to exceed 10 years.

[122] developed a model of the dust cloud where the dust is distributed along a single elliptical orbit. They demonstrated that such a model satisfies the observational constraints set out by the lack of infrared excess and duration of the dips, and that it can explain the long term dimming. According to this model the dust must transit the star at 0.05-0.6 AU. The ground based observations during 2015-2018 indicate that the long-term variability is also chromatic. The amplitude is largest in the B band, while the VRI flux amplitudes are progressively smaller by factors of 0.77 ± 0.05 , 0.50 ± 0.05 , and 0.31 ± 0.05 , respectively [123]. This implies that the dust particles causing the long-term variability must be about $0.1 \mu\text{m}$ in size. Such particles will be easily blown away and must be continuously replenished. The long-term variability (dimming) has a continuum of timescales ranging from almost a century, to decades, to years, and even down to a few months. It is most probably related to the shallow dip events and caused by the same phenomena. The net result is that the star has experienced about a 12% long-term dimming over the past century. This has serious implications for the amount of the dust that must be distributed along the elliptical orbit which now amounts to at least $10^{-3} M_{\oplus}$.

6.4 Possible explanation and models

There have been numerous models, ideas, and speculations proposed to explain the above mentioned behaviour. It is not possible to mention and discuss all the models here. An overview was presented in [124] and it concluded that intervening interstellar material (ISM) is a more plausible explanation than other natural models. The discoverers themselves discussed a number of possibilities and favoured a comet scenario. Apart from that it was proposed that KIC 8462852 might be undergoing a late heavy bombardment, but is only in its very early stages [106, 125]. It is also possible that the variability could be intrinsic to the star [126], or the dips might have been caused by matter in our Solar system [127]. According to [128] the secular dimming is the result of the inspiral of a planetary body or bodies into KIC 8462852, which took place $10 - 10^4$ yr ago. The discoverers also proposed that the dips observed with *Kepler* may be due to transits of less massive bodies placed on eccentric orbits by the Lidov-Kozai oscillations due to the outer M-dwarf companion. However, the predicted smooth decline in flux is not in agreement with the brightening episodes [119, 120], and the M-dwarf companion turned out not

to be associated with Boyajian’s star [104]. However, evidence is growing that the dipping phenomenon is due to circumstellar dust. In the next few sections we will mention three models that were developed to the point where they can be directly compared with the observations of the dip events.

6.4.1 A swarm of comets

This is the scenario favoured by the discoverers and developed by [129]. In this model the deep *Kepler* dips and long-term behaviour are due to transit of a large number (70-700) of comets. Such strings of comets are known from our Solar system so it is a natural explanation. An eccentric orbit has advantages. There is a high likelihood of the transits occurring near periastron and the material spends most of the time very far from the star so it can satisfy the IR limits as well as the dynamical constraints [122, 123]. These comets must have had a common progenitor. The models can fit the *Kepler* dips very well. Unfortunately, the model has a few drawbacks. (i) It cannot reproduce the D790 event because it is very smooth and has a slow ingress and a faster recovery, while the model features just the opposite behaviour with a steeper ingress and a slower egress. (ii) The symmetric triple dip, D1540, would require an accidental constellation of comets. However, there are two other events of this kind: D1210 and Skara Brae, and they would have to be the result of an accidental grouping of comets as well. (iii) Comets can hardly produce and continuously replenish $\gtrsim 10^{-3} M_{\oplus}$ of dust required to explain the long-term variability [123]. (iv) The model requires many free parameters (related to a large number of comets) and even a perfect fit does not mean that it is correct.

6.4.2 Massive asteroids wrapped in dust

This ‘recipe’ can be found in [101] but it was already considered in the discovery paper [11]. It is in many respects similar to the above mentioned scenario. According to this model there are a few massive asteroids or planetesimals surrounded by dust clouds orbiting and transiting the star on eccentric orbits. Obviously, the objects must have originated from a common progenitor as well. The orbit and the amount of the dust required to transit the star is similar to the previous model so it also satisfies the IR limits and the dynamical constraints [122, 123]. The difference is in the following. Instead of a large number of comets only four more massive objects are sufficient to explain the four major *Kepler* events. A massive object means that its gravity cannot be neglected, and it can retain a dust cloud within its Hill’s sphere (contrary to a comet). It naturally explains the smooth shape of the D790 event and produces a slower ingress and faster egress. The symmetric triple dips: D1540, D1210, and Skara Brae are no longer due to an accidental constellation of objects but rather single objects surrounded by dusty disks/rings. The massive asteroids can produce and replenish $\gtrsim 10^{-3} M_{\oplus}$ of dust to account for the long-term variability. It was demonstrated that if the objects were initially on exactly identical orbits, and

were massive enough, then they (and their dust clouds) would mutually interact and end up on a slightly different orbits. Even though the fits are not perfect, the model requires a small number of massive objects, and hence only a handful of free parameters. One can anticipate that massive asteroids are accompanied by a large number of smaller debris which would account for the smaller dips and long-term variability.

6.4.3 The Lord of the Rings

We hope the reader will not mind the ‘label’ above. The model was proposed by [130]. The authors noticed that one of the post *Kepler* dips (Skara Brae, the one that occurred around Aug 9, 2017) is very similar to the *Kepler* D1540 event, i.e., it is a symmetric triple dip with the central dip being the deepest. The similarity is indeed striking and the authors presume that it is the transit of the same body. This implies an orbital period of 1601 days. ‘The Lord’ is a dark and relatively massive object – a brown dwarf orbiting the star. It is accompanied by a ‘fellowship’ of about 9 rings which are about 0.2 AU across. With this model the authors were able to reproduce the Skara Brae and D1540 events very well. Apart from that the model explains a tentative 1600 day periodicity found in the long-term variability. The other dips observed by *Kepler* were not modelled but might be understood assuming transits of additional bodies (moons) related to the brown dwarf. The model makes a very precise and testable prediction. ‘The Return of the Lord’ should happen during Christmas on Dec 27, 2021.

A similar idea was presented earlier in [131]. The authors identified two strikingly similar events in the *Kepler* light curve which are approximately 0.1% deep and occurred at D216 and D1144. They show that these events could be explained by the occultation of the star by a giant ring system or by the transit of a string of half a dozen exocomets. These events occurred 928.25 days apart and the authors predict that the next event will occur between 3-8 October 2019.

More recent comparison and cross-correlation of *Kepler* dips and dips observed from the ground indicate a similar periodicity of 1574.4 days (4.31 yr) [132]. This period also explains a few other historical dimming events of the star in the past. It predicts the next return of the D790 event on Oct 17, 2019. We would like to comment that this idea presumes that the mutual gravitational interaction among the bodies orbiting the star must be negligible. It is not compatible with the brown-dwarf hypothesis.

It remains to be established whether these models are compatible with the long-term variability, infrared limits, and various other constraints including the dynamics of the system.

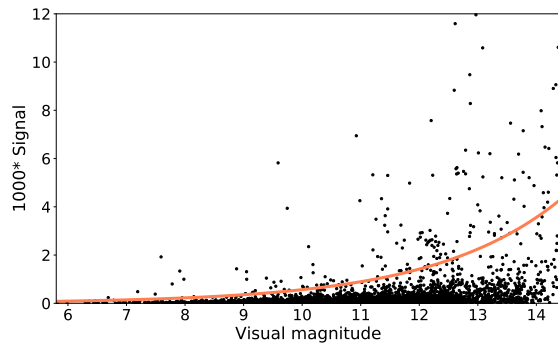
7 Ongoing and future space missions

Because *Kepler* played a pioneering role in the detection of a new class of ‘disintegrating’ objects, we shall briefly discuss ongoing and future space missions in order to present their potential for new discoveries of this particularly interesting class of objects.

7.1 TESS

TESS is a NASA space mission successfully launched in 2018 and planned for at least 2 years of operations [133, 134]. The aim of the *TESS* mission is the detection of several thousand exoplanets, mainly Neptune- and super Earth-sized. However, several hundred Jupiter-sized planet detections are expected as well. *TESS* is delivering precise photometry down to about 200 ppm which is sufficient to detect a transiting super-Earth ⁶. The first *TESS* planets were recently announced [135, 136]. There are many interesting objects discovered by *TESS*, such as a Neptune-sized planet HD 21749b with another, Earth-sized, planet HD 21749c in the same system [37] or the first *TESS* transiting brown dwarf [137]. Many of the *TESS* planets should be suitable for ground-based follow-up observations to detect exoplanetary atmospheres even with mid-sized telescopes [138] as shown in Figure 15. Furthermore, it is expected that *TESS* will detect additional interesting systems, and among those should be the types of disintegrating and dusty objects which we described in this review.

Fig. 15 Expected distribution of *TESS* planets with the orange line representing a detection threshold for mid-sized telescopes. Figure from [138] DOI: [10.1088/1538-3873/ab2143](https://doi.org/10.1088/1538-3873/ab2143). ©The Astronomical Society of the Pacific Reproduced by permission of IOP Publishing. All rights reserved.



⁶ <https://heasarc.gsfc.nasa.gov/docs/tess/observing-technical.html>

7.2 The PLATO space mission

The ESA M3 space mission PLATO (PLANetary Transits and Oscillations of stars) will be launched in 2026. The PLATO space mission will consist of 26 telescopes monitoring large portion of sky (about 50%) for transits with an unprecedented photometric accuracy of a few ppm [139]. The PLATO mission should find several thousand planetary candidates around one million bright stars from naked eye brightness to $V_{\text{mag}} = 11$. PLATO will be able to detect even an Earth-like planet on an Earth-like orbit among the Solar type stars. PLATO will also focus on asteroseismology of stars [140]. However, the PLATO mission will also contribute to many other fields of astrophysics ranging from variable star research to extragalactic objects [139]. The majority of the PLATO targets and candidates will be amenable to follow-up studies from the ground, thereby allowing for an exact determination of their masses and radii and thus allowing for their full characterization.

7.3 The ARIEL space mission

ARIEL, the Atmospheric Remote-sensing Infrared Exoplanet Large-survey, is an ESA M4 mission which will be launched in 2028 and it will be dedicated to unveiling the chemical composition of a sample of about 1000 selected transiting exoplanets [141]. ARIEL will be equipped with an off-axis Cassegrain telescope with an elliptical primary mirror of $1.1\text{-m} \times 0.7\text{-m}$. ARIEL will be capable of photometric monitoring in visible and infrared wavelengths between $0.50\text{-}0.55\ \mu\text{m}$, $0.8\text{-}1.0\ \mu\text{m}$ and $1.0\text{-}1.2\ \mu\text{m}$. A spectrograph with two medium resolving power channels of $1.95\text{-}3.9\ \mu\text{m}$ and $3.9\text{-}7.8\ \mu\text{m}$ and one low-resolution channel of $1.25\text{-}1.95\ \mu\text{m}$ will be available ⁷. The precision of ARIEL should be sufficient to detect the signature of exo-atmospheres with a precision of at least 10^{-4} relative to the star. The main targets will be hot (600 K and more) planets, and it is expected that species like H_2O , CO_2 , CH_4 , NH_3 , HCN or even metallic compounds such as TiO and VO will be detected and studied.

Acknowledgements The authors would like to thank Prof. Saul Rappaport for carefully reviewing the manuscript and his help with several sections. We acknowledge the ERASMUS+ project 'Per aspera ad astra simul' under number 2017-1-CZ01-KA203-035562 which funded the mobilities of the authors. Apart from that JB thanks for support the VEGA 2/0031/18 and APVV 15-0458 grants. PK acknowledges the support of GACR grant number 17-01752J. E.P is partly financed by the Spanish Ministry of Economics and Competitiveness through projects ESP2016-80435-C2-1-R and PGC2018-098153-B-C31.

⁷ <http://sci.esa.int/ariel/59798-summary/>

References

1. A. Wolszczan, D.A. Frail, *Nature***355**(6356), 145 (1992). DOI 10.1038/355145a0
2. M. Mayor, D. Queloz, *Nature***378**(6555), 355 (1995). DOI 10.1038/378355a0
3. D. Charbonneau, T.M. Brown, D.W. Latham, M. Mayor, *ApJ***529**(1), L45 (2000). DOI 10.1086/312457
4. G.Á. Bakos, *The HATNet and HATSouth Exoplanet Surveys* (2018), p. 111. DOI 10.1007/978-3-319-55333-7_111
5. J. Pepper, K.G. Stassun, B.S. Gaudi, *KELT: The Kilodegree Extremely Little Telescope, a Survey for Exoplanets Transiting Bright, Hot Stars* (2018), p. 128. DOI 10.1007/978-3-319-55333-7_128
6. A. Baglin, M. Auvergne, P. Barge, M. Deleuil, C. Catala, E. Michel, W. Weiss, COROT Team, in *The CoRoT Mission Pre-Launch Status - Stellar Seismology and Planet Finding, ESA Special Publication*, vol. 1306, ed. by M. Fridlund, A. Baglin, J. Lochard, L. Conroy (2006), *ESA Special Publication*, vol. 1306, p. 33
7. W.J. Borucki, D. Koch, G. Basri, N. Batalha, T. Brown, D. Caldwell, J. Caldwell, J. Christensen-Dalsgaard, W.D. Cochran, E. DeVore, E.W. Dunham, A.K. Dupree, T.N. Gautier, J.C. Geary, R. Gilliland, A. Gould, S.B. Howell, J.M. Jenkins, Y. Kondo, D.W. Latham, G.W. Marcy, S. Meibom, H. Kjeldsen, J.J. Lissauer, D.G. Monet, D. Morrison, D. Sasselov, J. Tarter, A. Boss, D. Brownlee, T. Owen, D. Buzasi, D. Charbonneau, L. Doyle, J. Fortney, E.B. Ford, M.J. Holman, S. Seager, J.H. Steffen, W.F. Welsh, J. Rowe, H. Anderson, L. Buchhave, D. Ciardi, L. Walkowicz, W. Sherry, E. Horch, H. Isaacson, M.E. Everett, D. Fischer, G. Torres, J.A. Johnson, M. Endl, P. MacQueen, S.T. Bryson, J. Dotson, M. Haas, J. Kolodziejczak, J. Van Cleve, H. Chandrasekaran, J.D. Twicken, E.V. Quintana, B.D. Clarke, C. Allen, J. Li, H. Wu, P. Tenenbaum, E. Verner, F. Bruhweiler, J. Barnes, A. Prsa, *Science***327**, 977 (2010). DOI 10.1126/science.1185402
8. W.J. Borucki, E. Agol, F. Fressin, L. Kaltenegger, J. Rowe, H. Isaacson, D. Fischer, N. Batalha, J.J. Lissauer, G.W. Marcy, D. Fabrycky, J.M. Désert, S.T. Bryson, T. Barclay, F. Bastien, A. Boss, E. Brugamyer, L.A. Buchhave, C. Burke, D.A. Caldwell, J. Carter, D. Charbonneau, J.R. Crepp, J. Christensen-Dalsgaard, J.L. Christiansen, D. Ciardi, W.D. Cochran, E. DeVore, L. Doyle, A.K. Dupree, M. Endl, M.E. Everett, E.B. Ford, J. Fortney, T.N. Gautier, J.C. Geary, A. Gould, M. Haas, C. Henze, A.W. Howard, S.B. Howell, D. Huber, J.M. Jenkins, H. Kjeldsen, R. Kolbl, J. Kolodziejczak, D.W. Latham, B.L. Lee, E. Lopez, F. Mullally, J.A. Orosz, A. Prsa, E.V. Quintana, R. Sanchis-Ojeda, D. Sasselov, S. Seader, A. Shporer, J.H. Steffen, M. Still, P. Tenenbaum, S.E. Thompson, G. Torres, J.D. Twicken, W.F. Welsh, J.N. Winn, *Science***340**(6132), 587 (2013). DOI 10.1126/science.1234702
9. J.N. Winn, R. Sanchis-Ojeda, S. Rappaport, *New A Rev.***83**, 37 (2018). DOI 10.1016/j.newar.2019.03.006
10. J.J. Lissauer, D.C. Fabrycky, E.B. Ford, W.J. Borucki, F. Fressin, G.W. Marcy, J.A. Orosz, J.F. Rowe, G. Torres, W.F. Welsh, N.M. Batalha, S.T. Bryson, L.A. Buchhave, D.A. Caldwell, J.A. Carter, D. Charbonneau, J.L. Christiansen, W.D. Cochran, J.M. Desert, E.W. Dunham, M.N. Fanelli, J.J. Fortney, I. Gautier, Thomas N., J.C. Geary, R.L. Gilliland, M.R. Haas, J.R. Hall, M.J. Holman, D.G. Koch, D.W. Latham, E. Lopez, S. McCauliff, N. Miller, R.C. Morehead, E.V. Quintana, D. Ragozzine, D. Sasselov, D.R. Short, J.H. Steffen, *Nature***470**(7332), 53 (2011). DOI 10.1038/nature09760
11. T.S. Boyajian, D.M. LaCourse, S.A. Rappaport, D. Fabrycky, D.A. Fischer, D. Gandolfi, G.M. Kennedy, H. Korhonen, M.C. Liu, A. Moor, K. Olah, K. Vida, M.C. Wyatt, W.M.J. Best, J. Brewer, F. Ciesla, B. Csák, H.J. Deeg, T.J. Dupuy, G. Handler, K. Heng, S.B. Howell, S.T. Ishikawa, J. Kovács, T. Kozakis, L. Kriskovics, J. Lehtinen, C. Lintott, S. Lynn, D. Nespral, S. Nikbakhsh, K. Schawinski, J.R. Schmitt, A.M. Smith, G. Szabo, R. Szabo, J. Viuhö, J. Wang, A. Weiksnar, M. Bosch, J.L. Connors, S. Goodman, G. Green, A.J. Hoekstra, T. Jebson, K.J. Jek, M.R. Omohundro, H.M. Schwengeler, A. Szweczyk, *MNRAS*(2016). DOI 10.1093/mnras/stw218

12. K.D. Colón, G. Zhou, A. Shporer, K.A. Collins, A. Bieryla, N. Espinoza, F. Murgas, P. Pattarakijwanich, S. Awiphan, J.D. Armstrong, J. Bailey, G. Barentsen, D. Bayliss, A. Chakpor, W.D. Cochran, V.S. Dhillon, K. Horne, M. Ireland, L. Kedziora-Chudczer, J.F. Kielkopf, S. Komonjinda, D.W. Latham, T.R. Marsh, D.E. Mkrtichian, E. Pallé, D. Rufolo, R. Sefako, C.G. Tinney, S. Wannawichian, S. Yuma, *AJ***156**(5), 227 (2018). DOI 10.3847/1538-3881/aae31b
13. R. van Lieshout, S.A. Rappaport, *Disintegrating Rocky Exoplanets* (2018), p. 15. DOI 10.1007/978-3-319-55333-7_15
14. C. Lovis, D. Fischer, *Radial Velocity Techniques for Exoplanets* (2010), pp. 27–53
15. J.T. Wright, *Radial Velocities as an Exoplanet Discovery Method* (2018), p. 4. DOI 10.1007/978-3-319-55333-7_4
16. A.P. Hatzes, E.W. Guenther, M. Endl, W.D. Cochran, M.P. Döllinger, A. Bedalov, *A&A***437**(2), 743 (2005). DOI 10.1051/0004-6361:20052850
17. J.N. Winn, arXiv e-prints arXiv:1001.2010 (2010)
18. A. Léger, D. Rouan, J. Schneider, P. Barge, M. Fridlund, B. Samuel, M. Ollivier, E. Guenther, M. Deleuil, H.J. Deeg, M. Auvergne, R. Alonso, S. Aigrain, A. Alapini, J.M. Almenara, A. Baglin, M. Barbieri, H. Bruntt, P. Bordé, F. Bouchy, J. Cabrera, C. Catala, L. Carone, S. Carpano, S. Csizmadia, R. Dvorak, A. Erikson, S. Ferraz-Mello, B. Foing, F. Fressin, D. Gandolfi, M. Gillon, P. Gondoin, O. Grasset, T. Guillot, A. Hatzes, G. Hébrard, L. Jorda, H. Lammer, A. Llebaria, B. Loeillet, M. Mayor, T. Mazeh, C. Moutou, M. Pätzold, F. Pont, D. Queloz, H. Rauer, S. Renner, R. Samadi, A. Shporer, C. Sotin, B. Tingley, G. Wuchterl, M. Adda, P. Agogu, T. Appourchaux, H. Ballans, P. Baron, T. Beaufort, R. Bellenger, R. Berlin, P. Bernardi, D. Blouin, F. Baudin, P. Bodin, L. Boisdard, L. Boit, F. Bonneau, S. Borzeix, R. Briet, J.T. Buey, B. Butler, D. Cailleau, R. Cautain, P.Y. Chabaud, S. Chainreuil, F. Chiavassa, V. Costes, V. Cuna Parrho, F. de Oliveira Fialho, M. Decaudin, J.M. Defise, S. Djalal, G. Epstein, G.E. Exil, C. Fauré, T. Fenouillet, A. Gaboriaud, A. Gallic, P. Gamet, P. Gavalda, E. Grolleau, R. Gruneisen, L. Gueguen, V. Guis, V. Guivarc'h, P. Guterman, D. Hallouard, J. Hasiba, F. Heuripeau, G. Huntzinger, H. Hustaix, C. Imad, C. Imbert, B. Johlander, M. Joutet, P. Journoud, F. Karioty, L. Kerjean, V. Lafaille, L. Lafond, T. Lam-Trong, P. Landiech, V. Lapeyriere, T. Larqué, P. Laudet, N. Lautier, H. Lecann, L. Lefevre, B. Leruyet, P. Levacher, A. Magnan, E. Mazy, F. Mertens, J.M. Mesnager, J.C. Meunier, J.P. Michel, W. Monjoin, D. Naudet, K. Nguyen-Kim, J.L. Orcesi, H. Ottacher, R. Perez, G. Peter, P. Plasson, J.Y. Plesseria, B. Pontet, A. Pradines, C. Quentin, J.L. Reynaud, G. Rolland, F. Rollenhagen, R. Romagnan, N. Russ, R. Schmidt, N. Schwartz, I. Sebbag, G. Sedes, H. Smit, M.B. Steller, W. Sunter, C. Surace, M. Tello, D. Tiphène, P. Toulouse, B. Ulmer, O. Vandermarq, E. Vergnault, A. Vuillemin, P. Zanatta, *A&A***506**(1), 287 (2009). DOI 10.1051/0004-6361/200911933
19. T. Barclay, J.F. Rowe, J.J. Lissauer, D. Huber, F. Fressin, S.B. Howell, S.T. Bryson, W.J. Chaplin, J.M. Désert, E.D. Lopez, G.W. Marcy, F. Mullally, D. Ragozzine, G. Torres, E.R. Adams, E. Agol, D. Barrado, S. Basu, T.R. Bedding, L.A. Buchhave, D. Charbonneau, J.L. Christiansen, J. Christensen-Dalsgaard, D. Ciardi, W.D. Cochran, A.K. Dupree, Y. Elsworth, M. Everett, D.A. Fischer, E.B. Ford, J.J. Fortney, J.C. Geary, M.R. Haas, R. Handberg, S. Hekker, C.E. Henze, E. Horch, A.W. Howard, R.C. Hunter, H. Isaacson, J.M. Jenkins, C. Karoff, S.D. Kawaler, H. Kjeldsen, T.C. Klaus, D.W. Latham, J. Li, J. Lillo-Box, M.N. Lund, M. Lundkvist, T.S. Metcalfe, A. Miglio, R.L. Morris, E.V. Quintana, D. Stello, J.C. Smith, M. Still, S.E. Thompson, *Nature***494**(7438), 452 (2013). DOI 10.1038/nature11914
20. D. Charbonneau, T.M. Brown, R.W. Noyes, R.L. Gilliland, *ApJ***568**(1), 377 (2002). DOI 10.1086/338770
21. A. Vidal-Madjar, A. Lecavelier des Etangs, J.M. Désert, G.E. Ballester, R. Ferlet, G. Hébrard, M. Mayor, *Nature***422**, 143 (2003). DOI 10.1038/nature01448
22. S. Redfield, M. Endl, W.D. Cochran, L. Koesterke, *ApJ***673**, L87 (2008). DOI 10.1086/527475
23. J.L. Bean, E. Miller-Ricci Kempton, D. Homeier, *Nature***468**(7324), 669 (2010). DOI 10.1038/nature09596
24. J.L. Bean, J.M. Désert, P. Kabath, B. Stalder, S. Seager, E. Miller-Ricci Kempton, Z.K. Berta, D. Homeier, S. Walsh, A. Seifahrt, *ApJ***743**(1), 92 (2011). DOI 10.1088/0004-637X/743/1/92

25. F. Murgas, G. Chen, E. Pallé, L. Nortmann, G. Nowak, *A&A***622**, A172 (2019). DOI 10.1051/0004-6361/201834063
26. G. Chen, E. Pallé, L. Welbanks, J. Prieto-Arranz, N. Madhusudhan, S. Gandhi, N. Casasayas-Barris, F. Murgas, L. Nortmann, N. Crouzet, H. Parviainen, D. Gandolfi, *A&A***616**, A145 (2018). DOI 10.1051/0004-6361/201833033
27. E. Sedaghati, H.M.J. Boffin, R.J. MacDonald, S. Gandhi, N. Madhusudhan, N.P. Gibson, M. Oshagh, A. Claret, H. Rauer, *Nature***549**(7671), 238 (2017). DOI 10.1038/nature23651
28. E. Pallé, M.R. Zapatero Osorio, A. García Muñoz, *ApJ***728**(1), 19 (2011). DOI 10.1088/0004-637X/728/1/19
29. N. Astudillo-Defru, P. Rojo, *A&A***557**, A56 (2013). DOI 10.1051/0004-6361/201219018
30. H.M. Cegla, C. Lovis, V. Bourrier, B. Beeck, C.A. Watson, F. Pepe, *A&A***588**, A127 (2016). DOI 10.1051/0004-6361/201527794
31. I.A.G. Snellen, S. Albrecht, E.J.W. de Mooij, R.S. Le Poole, *A&A***487**(1), 357 (2008). DOI 10.1051/0004-6361:200809762
32. A. Wyttenbach, D. Ehrenreich, C. Lovis, S. Udry, F. Pepe, *A&A***577**, A62 (2015). DOI 10.1051/0004-6361/201525729
33. J.V. Seidel, D. Ehrenreich, A. Wyttenbach, R. Allart, M. Lendl, L. Pino, V. Bourrier, H.M. Cegla, C. Lovis, D. Barrado, D. Bayliss, N. Astudillo-Defru, A. Deline, C. Fisher, K. Heng, R. Joseph, B. Lavie, C. Melo, F. Pepe, D. Ségransan, S. Udry, *A&A***623**, A166 (2019). DOI 10.1051/0004-6361/201834776
34. J. Žák, P. Kabáth, H.M.J. Boffin, V.D. Ivanov, M. Skarka, *AJ***158**(3), 120 (2019). DOI 10.3847/1538-3881/ab32ec
35. N. Casasayas-Barris, E. Palle, G. Nowak, F. Yan, L. Nortmann, F. Murgas, *A&A***608**, A135 (2017). DOI 10.1051/0004-6361/201731956
36. S.B. Howell, C. Sobeck, M. Haas, M. Still, T. Barclay, F. Mullally, J. Troeltzsch, S. Aigrain, S.T. Bryson, D. Caldwell, W.J. Chaplin, W.D. Cochran, D. Huber, G.W. Marcy, A. Miglio, J.R. Najita, M. Smith, J.D. Twicken, J.J. Fortney, *PASP***126**(938), 398 (2014). DOI 10.1086/676406
37. D. Dragomir, J. Teske, M.N. Günther, D. Ségransan, J.A. Burt, C.X. Huang, A. Vanderburg, E. Matthews, X. Dumusque, K.G. Stassun, J. Pepper, G.R. Ricker, R. Vanderspek, D.W. Latham, S. Seager, J.N. Winn, J.M. Jenkins, T. Beatty, F. Bouchy, T.M. Brown, R.P. Butler, D.R. Ciardi, J.D. Crane, J.D. Eastman, L. Fossati, J. Francis, B.J. Fulton, B.S. Gaudi, R.F. Goeke, D. James, T.C. Klaus, R.B. Kuhn, C. Lovis, M.B. Lund, S. McDermott, M. Paegert, F. Pepe, J.E. Rodriguez, L. Sha, S.A. Shectman, A. Shporer, R.J. Siverd, A. Garcia Soto, D.J. Stevens, J.D. Twicken, S. Udry, J. Villanueva, Steven, S.X. Wang, B. Wohler, X. Yao, Z. Zhan, *ApJ***875**(2), L7 (2019). DOI 10.3847/2041-8213/ab12ed
38. T.L. Campante, T. Barclay, J.J. Swift, D. Huber, V.Z. Adibekyan, W. Cochran, C.J. Burke, H. Isaacson, E.V. Quintana, G.R. Davies, V. Silva Aguirre, D. Ragozzine, R. Riddle, C. Baranec, S. Basu, W.J. Chaplin, J. Christensen-Dalsgaard, T.S. Metcalfe, T.R. Bedding, R. Handberg, D. Stello, J.M. Brewer, S. Hekker, C. Karoff, R. Kolbl, N.M. Law, M. Lundkvist, A. Miglio, J.F. Rowe, N.C. Santos, C. Van Laerhoven, T. Arentoft, Y.P. Elsworth, D.A. Fischer, S.D. Kawaler, H. Kjeldsen, M.N. Lund, G.W. Marcy, S.G. Sousa, A. Sozzetti, T.R. White, *ApJ***799**(2), 170 (2015). DOI 10.1088/0004-637X/799/2/170
39. N.M. Batalha, W.J. Borucki, S.T. Bryson, L.A. Buchhave, D.A. Caldwell, J. Christensen-Dalsgaard, D. Ciardi, E.W. Dunham, F. Fressin, I. Gautier, Thomas N., R.L. Gilliland, M.R. Haas, S.B. Howell, J.M. Jenkins, H. Kjeldsen, D.G. Koch, D.W. Latham, J.J. Lissauer, G.W. Marcy, J.F. Rowe, D.D. Sasselov, S. Seager, J.H. Steffen, G. Torres, G.S. Basri, T.M. Brown, D. Charbonneau, J. Christiansen, B. Clarke, W.D. Cochran, A. Dupree, D.C. Fabrycky, D. Fischer, E.B. Ford, J. Fortney, F.R. Girouard, M.J. Holman, J. Johnson, H. Isaacson, T.C. Klaus, P. Machalek, A.V. Moorehead, R.C. Morehead, D. Ragozzine, P. Tenenbaum, J. Twicken, S. Quinn, J. VanCleve, L.M. Walkowicz, W.F. Welsh, E. Devore, A. Gould, *ApJ***729**(1), 27 (2011). DOI 10.1088/0004-637X/729/1/27
40. F. Fressin, G. Torres, J.F. Rowe, D. Charbonneau, L.A. Rogers, S. Ballard, N.M. Batalha, W.J. Borucki, S.T. Bryson, L.A. Buchhave, D.R. Ciardi, J.M. Désert, C.D. Dressing, D.C.

- Fabrycky, E.B. Ford, I. Gautier, Thomas N., C.E. Henze, M.J. Holman, A. Howard, S.B. Howell, J.M. Jenkins, D.G. Koch, D.W. Latham, J.J. Lissauer, G.W. Marcy, S.N. Quinn, D. Ragozzine, D.D. Sasselov, S. Seager, T. Barclay, F. Mullally, S.E. Seader, M. Still, J.D. Twicken, S.E. Thompson, K. Uddin, *Nature***482**(7384), 195 (2012). DOI 10.1038/nature10780
41. P. Marigo, B. Aringer, *A&A***508**, 1539 (2009). DOI 10.1051/0004-6361/200912598
42. J. Budaj, M. Kocifaj, R. Salmeron, I. Hubeny, *MNRAS***454**, 2 (2015). DOI 10.1093/mnras/stv1711
43. J.A. Cardelli, G.C. Clayton, J.S. Mathis, *ApJ***345**, 245 (1989). DOI 10.1086/167900
44. J. Budaj, *A&A***557**, A72 (2013). DOI 10.1051/0004-6361/201220260
45. J. DeVore, S. Rappaport, R. Sanchis-Ojeda, K. Hoffman, J. Rowe, *MNRAS***461**, 2453 (2016). DOI 10.1093/mnras/stw1439
46. A. García Muñoz, J. Cabrera, *MNRAS***473**, 1801 (2018). DOI 10.1093/mnras/stx2428
47. M. Gillon, D.R. Anderson, A. Collier-Cameron, L. Delrez, C. Hellier, E. Jehin, M. Lendl, P.F.L. Maxted, F. Pepe, D. Pollacco, D. Queloz, D. Ségransan, A.M.S. Smith, B. Smalley, J. Southworth, A.H.M.J. Triaud, S. Udry, V. Van Grootel, R.G. West, *A&A***562**, L3 (2014). DOI 10.1051/0004-6361/201323014
48. J. Southworth, L. Mancini, S. Ciceri, J. Budaj, M. Dominik, R. Figuera Jaimes, T. Haugbølle, U.G. Jørgensen, A. Popovas, M. Rabus, S. Rahvar, C. von Essen, R.W. Schmidt, O. Wertz, K.A. Alsubai, V. Bozza, D.M. Bramich, S. Calchi Novati, G. D'Ago, T.C. Hinse, T. Henning, M. Hundertmark, D. Juncher, H. Korhonen, J. Skottfelt, C. Snodgrass, D. Starkey, J. Surdej, *MNRAS***447**, 711 (2015). DOI 10.1093/mnras/stu2394
49. C.F. Bohren, D.R. Huffman, *Absorption and scattering of light by small particles* (1983)
50. T. Henning, V.B. Il'In, N.A. Krivova, B. Michel, N.V. Voshchinnikov, *A&AS***136**, 405 (1999). DOI 10.1051/aas:1999222
51. C. Jäger, J. Dorschner, H. Mutschke, T. Posch, T. Henning, *A&A***408**, 193 (2003). DOI 10.1051/0004-6361:20030916
52. H. Kimura, I. Mann, D.A. Biesecker, E.K. Jessberger, *Icarus***159**, 529 (2002). DOI 10.1006/icar.2002.6940
53. R. van Lieshout, M. Min, C. Dominik, *A&A***572**, A76 (2014). DOI 10.1051/0004-6361/201424876
54. J. Dorschner, B. Begemann, T. Henning, C. Jaeger, H. Mutschke, *A&A***300**, 503 (1995)
55. M. Asplund, N. Grevesse, A.J. Sauval, P. Scott, *ARA&A***47**, 481 (2009). DOI 10.1146/annurev.astro.46.060407.145222
56. A. Burrows, D. Sudarsky, I. Hubeny, *ApJ***640**, 1063 (2006). DOI 10.1086/500293
57. S. Rappaport, A. Levine, E. Chiang, I. El Mellah, J. Jenkins, B. Kalomeni, E.S. Kite, M. Koton, L. Nelson, L. Rousseau-Nepton, K. Tran, *ApJ***752**, 1 (2012). DOI 10.1088/0004-637X/752/1/1
58. E. Schlawin, T. Hirano, H. Kawahara, J. Teske, E.M. Green, B.V. Rackham, J. Fraine, R. Bushra, *AJ***156**, 281 (2018). DOI 10.3847/1538-3881/aab32
59. H. Kawahara, T. Hirano, K. Kurosaki, Y. Ito, M. Ikoma, *ApJ***776**, L6 (2013). DOI 10.1088/2041-8205/776/1/L6
60. B. Croll, S. Rappaport, J. DeVore, R.L. Gilliland, J.R. Crepp, A.W. Howard, K.M. Star, E. Chiang, A.M. Levine, J.M. Jenkins, L. Albert, A.S. Bonomo, J.J. Fortney, H. Isaacson, *ApJ***786**, 100 (2014). DOI 10.1088/0004-637X/786/2/100
61. K. Masuda, T. Hirano, H. Kawahara, B. Sato, *Research Notes of the American Astronomical Society* **2**(1), 50 (2018). DOI 10.3847/2515-5172/aaba12
62. D. Perez-Becker, E. Chiang, *MNRAS***433**, 2294 (2013). DOI 10.1093/mnras/stt895
63. E.H.L. Bodman, J.T. Wright, S.J. Desch, C.M. Lisse, *AJ***156**, 173 (2018). DOI 10.3847/1538-3881/aadc60
64. A.R. Ridden-Harper, C.U. Keller, M. Min, R. van Lieshout, I.A.G. Snellen, *A&A***618**, A97 (2018). DOI 10.1051/0004-6361/201731947
65. T.I.M. van Werkhoven, M. Brogi, I.A.G. Snellen, C.U. Keller, *A&A***561**, A3 (2014). DOI 10.1051/0004-6361/201322398
66. B. Croll, S. Rappaport, A.M. Levine, *MNRAS***449**, 1408 (2015). DOI 10.1093/mnras/stv297

67. E. Schlawin, T. Herter, M. Zhao, J.K. Teske, H. Chen, *ApJ***826**, 156 (2016). DOI 10.3847/0004-637X/826/2/156
68. R. van Lieshout, M. Min, C. Dominik, M. Brogi, T. de Graaff, S. Hekker, M. Kama, C.U. Keller, A. Ridden-Harper, T.I.M. van Werkhoven, *A&A***596**, A32 (2016). DOI 10.1051/0004-6361/201629250
69. S. Rappaport, T. Barclay, J. DeVore, J. Rowe, R. Sanchis-Ojeda, M. Still, *ApJ***784**, 40 (2014). DOI 10.1088/0004-637X/784/1/40
70. M. Brogi, C.U. Keller, M. de Juan Ovelar, M.A. Kenworthy, R.J. de Kok, M. Min, I.A.G. Snellen, *A&A***545**, L5 (2012). DOI 10.1051/0004-6361/201219762
71. J.J. Bochinski, C.A. Haswell, T.R. Marsh, V.S. Dhillon, S.P. Littlefair, *ApJ***800**, L21 (2015). DOI 10.1088/2041-8205/800/2/L21
72. R. Sanchis-Ojeda, S. Rappaport, E. Pall , L. Delrez, J. DeVore, D. Gandolfi, A. Fukui, I. Ribas, K.G. Stassun, S. Albrecht, F. Dai, E. Gaidos, M. Gillon, T. Hirano, M. Holman, A.W. Howard, H. Isaacson, E. Jehin, M. Kuzuhara, A.W. Mann, G.W. Marcy, P.A. Miles-P ez, P. Monta  es-Rodr guez, F. Murgas, N. Narita, G. Nowak, M. Onitsuka, M. Paegert, V. Van Eylen, J.N. Winn, L. Yu, *ApJ***812**, 112 (2015). DOI 10.1088/0004-637X/812/2/112
73. K.D. Col n, G. Zhou, A. Shporer, K.A. Collins, A. Bieryla, N. Espinoza, F. Murgas, P. Pattarakijwanich, S. Awiphan, J.D. Armstrong, J. Bailey, G. Barentsen, D. Bayliss, A. Chakpor, W.D. Cochran, V.S. Dhillon, K. Horne, M. Ireland, L. Kedziora-Chudczer, J.F. Kielkopf, S. Komonjinda, D.W. Latham, T.R. Marsh, D.E. Mkrtichian, E. Pall , D. Rufolo, R. Sefako, C.G. Tinney, S. Wannawichian, S. Yuma, *AJ***156**, 227 (2018). DOI 10.3847/1538-3881/aae31b
74. E. Gaidos, T. Hirano, M. Ansdell, *MNRAS*(2019). DOI 10.1093/mnras/stz693
75. A. Vanderburg, J.A. Johnson, S. Rappaport, A. Bieryla, J. Irwin, J.A. Lewis, D. Kipping, W.R. Brown, P. Dufour, D.R. Ciardi, R. Angus, L. Schaefer, D.W. Latham, D. Charbonneau, C. Beichman, J. Eastman, N. McCrady, R.A. Wittenmyer, J.T. Wright, *Nature***526**(7574), 546 (2015). DOI 10.1038/nature15527
76. B. Zuckerman, C. Melis, B. Klein, D. Koester, M. Jura, *ApJ***722**, 725 (2010). DOI 10.1088/0004-637X/722/1/725
77. D. Koester, B.T. G nsicke, J. Farihi, *A&A***566**, A34 (2014). DOI 10.1051/0004-6361/201423691
78. M. Jura, *ApJ***584**(2), L91 (2003). DOI 10.1086/374036
79. M. Jura, J. Farihi, B. Zuckerman, *ApJ***663**(2), 1285 (2007). DOI 10.1086/518767
80. M. Kilic, T. von Hippel, S.K. Leggett, D.E. Winget, *ApJ***646**(1), 474 (2006). DOI 10.1086/504682
81. B. Croll, P.A. Dalba, A. Vanderburg, J. Eastman, S. Rappaport, J. DeVore, A. Bieryla, P.S. Muirhead, E. Han, D.W. Latham, T.G. Beatty, R.A. Wittenmyer, J.T. Wright, J.A. Johnson, N. McCrady, *ApJ***836**(1), 82 (2017). DOI 10.3847/1538-4357/836/1/82
82. S. Rappaport, B.L. Gary, A. Vanderburg, S. Xu, D. Pooley, K. Mukai, *MNRAS***474**, 933 (2018). DOI 10.1093/mnras/stx2663
83. R. Alonso, S. Rappaport, H.J. Deeg, E. Palle, *A&A***589**, L6 (2016). DOI 10.1051/0004-6361/201628511
84. P. Izquierdo, P. Rodr guez-Gil, B.T. G nsicke, A.J. Mustill, O. Toloza, P.E. Tremblay, M. Wyatt, P. Chote, S. Eggl, J. Farihi, D. Koester, W. Lyra, C.J. Manser, T.R. Marsh, E. Pall , R. Raddi, D. Veras, E. Villaver, S. Portegies Zwart, *MNRAS***481**(1), 703 (2018). DOI 10.1093/mnras/sty2315
85. G. Zhou, L. Kedziora-Chudczer, J. Bailey, J.P. Marshall, D.D.R. Bayliss, C. Stockdale, P. Nelson, T.G. Tan, J.E. Rodriguez, C.G. Tinney, D. Dragomir, K. Colon, A. Shporer, J. Bento, R. Sefako, K. Horne, W. Cochran, *MNRAS***463**, 4422 (2016). DOI 10.1093/mnras/stw2286
86. S. Xu, S. Rappaport, R. van Lieshout, A. Vanderburg, B. Gary, N. Hallakoun, V.D. Ivanov, M.C. Wyatt, J. DeVore, D. Bayliss, J. Bento, A. Bieryla, A. Cameron, J.M. Cann, B. Croll, K.A. Collins, P.A. Dalba, J. Debes, D. Doyle, P. Dufour, J. Ely, N. Espinoza, M.D. J ner, M. Jura, T. Kaye, J.L. McClain, P. Muirhead, E. Palle, P.A. Panka, J. Provencal, S. Randall, J.E. Rodriguez, J. Scarborough, R. Sefako, A. Shporer, W. Strickland, G. Zhou, B. Zuckerman, *MNRAS***474**(4), 4795 (2018). DOI 10.1093/mnras/stx3023

87. S. Xu, N. Hallakoun, B. Gary, P.A. Dalba, J. Debes, P. Dufour, M. Fortin-Archambault, A. Fukui, M.A. Jura, B. Klein, N. Kusakabe, P.S. Muirhead, N. Narita, A. Steele, K.Y.L. Su, A. Vanderburg, N. Watanabe, Z. Zhan, B. Zuckerman, *AJ***157**(6), 255 (2019). DOI 10.3847/1538-3881/ab1b36
88. S. Rappaport, B.L. Gary, T. Kaye, A. Vanderburg, B. Croll, P. Benni, J. Foote, *MNRAS***458**, 3904 (2016). DOI 10.1093/mnras/stw612
89. B.T. Gänsicke, A. Aungwerojwit, T.R. Marsh, V.S. Dhillon, D.I. Sahman, D. Veras, J. Farihi, P. Chote, R. Ashley, S. Arjyotha, S. Rattanasoon, S.P. Littlefair, D. Pollacco, M.R. Burleigh, *ApJ***818**, L7 (2016). DOI 10.3847/2041-8205/818/1/L7
90. S. Xu, M. Jura, P. Dufour, B. Zuckerman, *ApJ***816**, L22 (2016). DOI 10.3847/2041-8205/816/2/L22
91. S. Redfield, J. Farihi, P.W. Cauley, S.G. Parsons, B.T. Gänsicke, G.M. Duvvuri, *ApJ***839**, 42 (2017). DOI 10.3847/1538-4357/aa68a0
92. A. Vanderburg, S.A. Rappaport, *Transiting Disintegrating Planetary Debris Around WD 1145+017* (2018), p. 37. DOI 10.1007/978-3-319-55333-7_37
93. Z. Vanderbosch, J.J. Hermes, E. Dennyhy, B.H. Dunlap, P. Izquierdo, P.E. Tremblay, P.B. Cho, B.T. Gänsicke, K.J. Bell, M.H. Montgomery, D.E. Winget, arXiv e-prints arXiv:1908.09839 (2019)
94. A. Lecavelier Des Etangs, A. Vidal-Madjar, R. Ferlet, *A&A***343**, 916 (1999)
95. S. Rappaport, A. Vanderburg, T. Jacobs, D. LaCourse, J. Jenkins, A. Kraus, A. Rizzuto, D.W. Latham, A. Bieryla, M. Lazarevic, A. Schmitt, *MNRAS***474**, 1453 (2018). DOI 10.1093/mnras/stx2735
96. G.M. Kennedy, G. Hope, S.T. Hodgkin, M.C. Wyatt, *MNRAS***482**, 5587 (2019). DOI 10.1093/mnras/sty3049
97. S. Zieba, K. Zwintz, M.A. Kenworthy, G.M. Kennedy, *A&A***625**, L13 (2019). DOI 10.1051/0004-6361/201935552
98. M. Ansdell, E. Gaidos, T.L. Jacobs, A. Mann, C.F. Manara, G.M. Kennedy, A. Vanderburg, M. Kenworthy, T. Hirano, D.M. LaCourse, C. Hedges, A. Frasca, *MNRAS***483**, 3579 (2019). DOI 10.1093/mnras/sty3289
99. S. Rappaport, A. Vanderburg, M.H. Kristiansen, M.R. Omohundro, H.M. Schwengeler, I.A. Terentev, F. Dai, K. Masuda, T.L. Jacobs, D. LaCourse, D.W. Latham, A. Bieryla, C.L. Hedges, J. Dittmann, G. Barentsen, W. Cochran, M. Endl, J.M. Jenkins, A. Mann, *MNRAS***488**, 2455 (2019). DOI 10.1093/mnras/stz1772
100. S. Rappaport, G. Zhou, A. Vanderburg, A. Mann, M.H. Kristiansen, K. Oláh, T.L. Jacobs, E. Newton, M.R. Omohundro, D. LaCourse, H.M. Schwengeler, I.A. Terentev, D.W. Latham, A. Bieryla, M. Soares-Furtado, L.G. Bouma, M.J. Ireland, J. Irwin, *MNRAS***485**, 2681 (2019). DOI 10.1093/mnras/stz537
101. L. Neslušan, J. Budaj, *A&A***600**, A86 (2017). DOI 10.1051/0004-6361/201629344
102. M.J. Martínez González, C. González-Fernández, A. Asensio Ramos, H. Socas-Navarro, C. Westendorp Plaza, T.S. Boyajian, J.T. Wright, A. Collier Cameron, J.I. González Hernández, G. Holgado, G.M. Kennedy, T. Masseron, E. Molinari, J. Saario, S. Simón-Díaz, B. Toledo-Adrón, *MNRAS***486**, 236 (2019). DOI 10.1093/mnras/stz850
103. V.V. Makarov, A. Goldin, *ApJ***833**, 78 (2016). DOI 10.3847/1538-4357/833/1/78
104. D.P. Clemens, K. Maheshwari, R. Jagani, J. Montgomery, A.M. El Batal, T.G. Ellis, J.T. Wright, *ApJ***856**, L8 (2018). DOI 10.3847/2041-8213/aab492
105. M. Marengo, A. Hulsebus, S. Willis, *ApJ***814**, L15 (2015). DOI 10.1088/2041-8205/814/1/L15
106. C.M. Lisse, M.L. Sitko, M. Marengo, *ApJ***815**, L27 (2015). DOI 10.1088/2041-8205/815/2/L27
107. M.A. Thompson, P. Scicluna, F. Kemper, J.E. Geach, M.M. Dunham, O. Morata, S. Ertel, P.T.P. Ho, J. Dempsey, I. Coulson, G. Petitpas, L.E. Kristensen, *MNRAS***458**, L39 (2016). DOI 10.1093/mnras/slz008
108. T.S. Boyajian, R. Alonso, A. Ammerman, D. Armstrong, A. Asensio Ramos, K. Barkaoui, T.G. Beatty, Z. Benkhaldoun, P. Benni, R.O. Bentley, et al., *ApJ***853**, L8 (2018). DOI 10.3847/2041-8213/aaa405

109. I.A. Steele, C.M. Copperwheat, H.E. Jermak, G.M. Kennedy, G.P. Lamb, *MNRAS***473**, L26 (2018). DOI 10.1093/mnras/slx145
110. E. Bodman, J. Wright, T. Boyajian, T. Ellis, arXiv e-prints (2018)
111. H.J. Deeg, R. Alonso, D. Nespral, T.S. Boyajian, *A&A***610**, L12 (2018). DOI 10.1051/0004-6361/201732453
112. B.E. Schaefer, *ApJ***822**, L34 (2016). DOI 10.3847/2041-8205/822/2/L34
113. M. Hippke, D. Angerhausen, M.B. Lund, J. Pepper, K.G. Stassun, *ApJ***825**, 73 (2016). DOI 10.3847/0004-637X/825/1/73
114. M. Hippke, P. Kroll, F. Matthalai, D. Angerhausen, T. Tuvikene, K.G. Stassun, E. Roshchina, T. Vasileva, I. Izmailov, N.N. Samus, E.N. Pastukhova, I. Bryukhanov, M.B. Lund, *ApJ***837**, 85 (2017). DOI 10.3847/1538-4357/aa615d
115. M. Castelaz, T. Barker, *Journal of the American Association of Variable Star Observers (JAAVSO)* **46**, 33 (2018)
116. B.T. Montet, J.D. Simon, *ApJ***830**, L39 (2016). DOI 10.3847/2041-8205/830/2/L39
117. J.R.A. Davenport, K.R. Covey, R.W. Clarke, Z. Laycock, S.W. Fleming, T.S. Boyajian, B.T. Montet, B. Shiao, C.C. Million, D.J. Wilson, M. Olmedo, E.E. Mamajek, D. Olmedo, M. Chávez, E. Bertone, *ApJ***853**, 130 (2018). DOI 10.3847/1538-4357/aaa413
118. H.Y.A. Meng, G. Rieke, F. Dubois, G. Kennedy, M. Marengo, M. Siegel, K. Su, N. Trueba, M. Wyatt, T. Boyajian, C.M. Lisse, L. Logie, S. Rau, S. Vanaverbeke, *ApJ***847**, 131 (2017). DOI 10.3847/1538-4357/aa899c
119. B. Gary, R. Bourne, *Research Notes of the American Astronomical Society* **1**(1), 22 (2017). DOI 10.3847/2515-5172/aa9bdd
120. J.D. Simon, B.J. Shappee, G. Pojmański, B.T. Montet, C.S. Kochanek, J. van Saders, T.W.S. Holoien, A.A. Henden, *ApJ***853**, 77 (2018). DOI 10.3847/1538-4357/aaa0c1
121. M. Hippke, D. Angerhausen, *ApJ***854**, L11 (2018). DOI 10.3847/2041-8213/aaab44
122. M.C. Wyatt, R. van Lieshout, G.M. Kennedy, T.S. Boyajian, *MNRAS***473**, 5286 (2018). DOI 10.1093/mnras/stx2713
123. B.E. Schaefer, R.O. Bentley, T.S. Boyajian, P.H. Coker, S. Dvorak, F. Dubois, E. Erdelyi, T. Ellis, K. Graham, B.G. Harris, J.E. Hall, R. James, S.J. Johnston, G. Kennedy, L. Logie, K.M. Nugent, A. Oksanen, J.J. Ott, S. Rau, S. Vanaverbeke, R. van Lieshout, M. Wyatt, *MNRAS***481**, 2235 (2018). DOI 10.1093/mnras/sty1644
124. J.T. Wright, S. Sigurdsson, *ApJ***829**, L3 (2016). DOI 10.3847/2041-8205/829/1/L3
125. K.M. Punzi, J.H. Kastner, C. Melis, B. Zuckerman, C. Pilachowski, L. Gingerich, T. Knapp, *AJ***155**, 33 (2018). DOI 10.3847/1538-3881/aa9524
126. P. Foukal, *ApJ***842**, L3 (2017). DOI 10.3847/2041-8213/aa740f
127. J.I. Katz, *MNRAS***471**, 3680 (2017). DOI 10.1093/mnras/stx1876
128. B.D. Metzger, K.J. Shen, N. Stone, *MNRAS***468**, 4399 (2017). DOI 10.1093/mnras/stx823
129. E.H.L. Bodman, A. Quillen, *ApJ***819**, L34 (2016). DOI 10.3847/2041-8205/819/2/L34
130. R. Bourne, B.L. Gary, A. Plakhov, *MNRAS***475**, 5378 (2018). DOI 10.1093/mnras/sty097
131. F. Kiefer, A. Lecavelier des Étangs, A. Vidal-Madjar, G. Hébrard, V. Bourrier, P.A. Wilson, *A&A***608**, A132 (2017). DOI 10.1051/0004-6361/201731306
132. G. Sacco, L.D. Ngo, J. Modolo, *Journal of the American Association of Variable Star Observers (JAAVSO)* **46**, 14 (2018)
133. G.R. Ricker, J.N. Winn, R. Vanderspek, D.W. Latham, G.Á. Bakos, J.L. Bean, Z.K. Berta-Thompson, T.M. Brown, L. Buchhave, N.R. Butler, R.P. Butler, W.J. Chaplin, D. Charbonneau, J. Christensen-Dalsgaard, M. Clampin, D. Deming, J. Doty, N. De Lee, C. Dressing, E.W. Dunham, M. Endl, F. Fressin, J. Ge, T. Henning, M.J. Holman, A.W. Howard, S. Ida, J. Jenkins, G. Jernigan, J.A. Johnson, L. Kaltenegger, N. Kawai, H. Kjeldsen, G. Laughlin, A.M. Levine, D. Lin, J.J. Lissauer, P. MacQueen, G. Marcy, P.R. McCullough, T.D. Morton, N. Narita, M. Paegert, E. Palle, F. Pepe, J. Pepper, A. Quirrenbach, S.A. Rinehart, D. Sasselov, B. Sato, S. Seager, A. Sozzetti, K.G. Stassun, P. Sullivan, A. Szentgyorgyi, G. Torres, S. Udry, J. Villaseñor, in *Society of Photo-Optical Instrumentation Engineers (SPIE) Conference Series, Society of Photo-Optical Instrumentation Engineers (SPIE) Conference Series*, vol. 9143 (2014), *Society of Photo-Optical Instrumentation Engineers (SPIE) Conference Series*, vol. 9143, p. 20. DOI 10.1117/12.2063489

134. G.R. Ricker, J.N. Winn, R. Vanderspek, D.W. Latham, G.Á. Bakos, J.L. Bean, Z.K. Berta-Thompson, T.M. Brown, L. Buchhave, N.R. Butler, R.P. Butler, W.J. Chaplin, D. Charbonneau, J. Christensen-Dalsgaard, M. Clampin, D. Deming, J. Doty, N. De Lee, C. Dressing, E.W. Dunham, M. Endl, F. Fressin, J. Ge, T. Henning, M.J. Holman, A.W. Howard, S. Ida, J.M. Jenkins, G. Jernigan, J.A. Johnson, L. Kaltenegger, N. Kawai, H. Kjeldsen, G. Laughlin, A.M. Levine, D. Lin, J.J. Lissauer, P. MacQueen, G. Marcy, P.R. McCullough, T.D. Morton, N. Narita, M. Paegert, E. Palles, F. Pepe, J. Pepper, A. Quirrenbach, S.A. Rinehart, D. Sasselov, B. Sato, S. Seager, A. Sozzetti, K.G. Stassun, P. Sullivan, A. Szentgyorgyi, G. Torres, S. Udry, J. Villaseñor, *Journal of Astronomical Telescopes, Instruments, and Systems* **1**(1), 014003 (2015). DOI 10.1117/1.JATIS.1.1.014003
135. D. Gandolfi, O. Barragán, J.H. Livingston, M. Fridlund, A.B. Justesen, S. Redfield, L. Fossati, S. Mathur, S. Grziwa, J. Cabrera, R.A. García, C.M. Persson, V. Van Eylen, A.P. Hatzes, D. Hidalgo, S. Albrecht, L. Bugnet, W.D. Cochran, S. Csizmadia, H. Deeg, P. Eigmüller, M. Endl, A. Erikson, M. Esposito, E. Guenther, J. Korth, R. Luque, P. Montañes Rodríguez, D. Nespral, G. Nowak, M. Pätzold, J. Prieto-Arranz, *A&A* **619**, L10 (2018). DOI 10.1051/0004-6361/201834289
136. C.X. Huang, J. Burt, A. Vanderburg, M.N. Günther, A. Shporer, J.A. Dittmann, J.N. Winn, R. Wittenmyer, L. Sha, S.R. Kane, G.R. Ricker, R.K. Vanderspek, D.W. Latham, S. Seager, J.M. Jenkins, D.A. Caldwell, K.A. Collins, N. Guerrero, J.C. Smith, S.N. Quinn, S. Udry, F. Pepe, F. Bouchy, D. Ségransan, C. Lovis, D. Ehrenreich, M. Marmier, M. Mayor, B. Wöhlér, K. Haworth, E.H. Morgan, M. Fausnaugh, D.R. Ciardi, J. Christiansen, D. Charbonneau, D. Dragomir, D. Deming, A. Glidden, A.M. Levine, P.R. McCullough, L. Yu, N. Narita, T. Nguyen, T. Morton, J. Pepper, A. Pál, J.E. Rodríguez, K.G. Stassun, G. Torres, A.R. Sozzetti, J.P. Doty, J. Christensen-Dalsgaard, G. Laughlin, M. Clampin, J.L. Bean, L.A. Buchhave, G.Á. Bakos, B. Sato, S. Ida, L. Kaltenegger, E. Palles, D. Sasselov, R.P. Butler, J. Lissauer, J. Ge, S.A. Rinehart, *ApJ* **868**(2), L39 (2018). DOI 10.3847/2041-8213/aaef91
137. J. Šubjak, R. Sharma, T.W. Carmichael, M.C. Johnson, E.J. Gonzales, E. Matthews, H.M.J. Boffin, R. Brahm, P. Chaturvedi, A. Chakraborty, D.R. Ciardi, K.A. Collins, M. Esposito, M. Fridlund, T. Gan, D. Gandolfi, R.A. García, E. Guenther, A. Hatzes, D.W. Latham, C.M. Persson, H.M. Relles, J.E. Schlieder, T. Barclay, C. Dressing, I. Crossfield, A.W. Howard, F. Rodler, G. Zhou, S.N. Quinn, G.A. Esquerdo, M.L. Calkins, P. Berlind, K.G. Stassun, S. Albrecht, R. Alonso Sobrino, P. Beck, M. Blažek, J. Cabrera, I. Carleo, W.D. Cochran, S. Csizmadia, F. Dai, H.J. Deeg, J.P. de Leon, P. Eigmüller, M. Endl, A. Erikson, A. Fukui, I. Georgieva, L. González-Cuesta, S. Grziwa, D. Hidalgo, T. Hirano, M. Hjorth, E. Knudstrup, J. Korth, K.W.F. Lam, J.H. Livingston, M.N. Lund, R. Luque, S. Mathur, P. Montañes Rodríguez, F. Murgas, N. Narita, D. Nespral, P. Niraula, G. Nowak, E. Pallé, M. Pätzold, J. Prieto-Arranz, H. Rauer, S. Redfield, I. Ribas, M. Skarka, A.M.S. Smith, M. Špoková, V. Van Eylen, P. Kabáth, arXiv e-prints arXiv:1909.07984 (2019)
138. P. Kabáth, J. Žák, H.M.J. Boffin, V.D. Ivanov, D. Jones, M. Skarka, *PASP* **131**(1002), 085001 (2019). DOI 10.1088/1538-3873/ab2143
139. H. Rauer, C. Catala, C. Aerts, T. Appourchaux, W. Benz, A. Brandeker, J. Christensen-Dalsgaard, M. Deleuil, L. Gizon, M.J. Goupil, M. Güdel, E. Janot-Pacheco, M. Mas-Hesse, I. Pagano, G. Piotto, D. Pollacco, C. Santos, A. Smith, J.C. Suárez, R. Szabó, S. Udry, V. Adibekyan, Y. Alibert, J.M. Almenara, P. Amaro-Seoane, M.A.v. Eiff, M. Asplund, E. Antonello, S. Barnes, F. Baudin, K. Belkacem, M. Bergemann, G. Bihain, A.C. Birch, X. Bonfils, I. Boisse, A.S. Bonomo, F. Borsa, I.M. Brandão, E. Brocato, S. Brun, M. Burleigh, R. Burston, J. Cabrera, S. Cassisi, W. Chaplin, S. Charpinet, C. Chiappini, R.P. Church, S. Csizmadia, M. Cunha, M. Damasso, M.B. Davies, H.J. Deeg, R.F. Díaz, S. Dreizler, C. Dreyer, P. Eggenberger, D. Ehrenreich, P. Eigmüller, A. Erikson, R. Farmer, S. Feltzing, F. de Oliveira Fialho, P. Figueira, T. Forveille, M. Fridlund, R.A. García, P. Giommi, G. Giuffrida, M. Godolt, J. Gomes da Silva, T. Granzer, J.L. Grenfell, A. Grottsch-Noels, E. Günther, C.A. Haswell, A.P. Hatzes, G. Hébrard, S. Hekker, R. Helled, K. Heng, J.M. Jenkins, A. Johansen, M.L. Khodachenko, K.G. Kislyakova, W. Kley, U. Kolb, N. Krivova, F. Kupka, H. Lammer, A.F. Lanza, Y. Lebreton, D. Magrin, P. Marcos-Arenal, P.M. Marrese, J.P. Marques, J. Martins,

- S. Mathis, S. Mathur, S. Messina, A. Miglio, J. Montalban, M. Montalto, M.J.P.F.G. Monteiro, H. Moradi, E. Moravveji, C. Mordasini, T. Morel, A. Mortier, V. Nascimbeni, R.P. Nelson, M.B. Nielsen, L. Noack, A.J. Norton, A. Ofir, M. Oshagh, R.M. Ouazzani, P. Pápics, V.C. Parro, P. Petit, B. Plez, E. Poretti, A. Quirrenbach, R. Ragazzoni, G. Raimondo, M. Rainer, D.R. Reese, R. Redmer, S. Reffert, B. Rojas-Ayala, I.W. Roxburgh, S. Salmon, A. Sarterne, J. Schneider, J. Schou, S. Schuh, H. Schunker, A. Silva-Valio, R. Silvotti, I. Skillen, I. Snellen, F. Sohl, S.G. Sousa, A. Sozzetti, D. Stello, K.G. Strassmeier, M. Švanda, G.M. Szabó, A. Tkachenko, D. Valencia, V. Van Grootel, S.D. Vauclair, P. Ventura, F.W. Wagner, N.A. Walton, J. Weingrill, S.C. Werner, P.J. Wheatley, K. Zwintz, *Experimental Astronomy* **38**, 249 (2014). DOI 10.1007/s10686-014-9383-4
140. M. Goupil, in *European Physical Journal Web of Conferences, European Physical Journal Web of Conferences*, vol. 160 (2017), *European Physical Journal Web of Conferences*, vol. 160, p. 01003. DOI 10.1051/epjconf/201716001003
141. G. Tinetti, J.P. Beaulieu, T. Henning, M. Meyer, G. Micela, I. Ribas, D. Stam, M. Swain, O. Krause, M. Ollivier, E. Pace, B. Swinyard, A. Aylward, R. van Boekel, A. Coradini, T. Encrenaz, I. Snellen, M.R. Zapatero-Osorio, J. Bouwman, J.Y.K. Cho, V. Coudé de Foresto, T. Guillot, M. Lopez-Morales, I. Mueller-Wodarg, E. Palle, F. Selsis, A. Sozzetti, P.A.R. Ade, N. Achilleos, A. Adriani, C.B. Agnor, C. Afonso, C. Allende Prieto, G. Bakos, R.J. Barber, M. Barlow, V. Batista, P. Bernath, B. Bézard, P. Bordé, L.R. Brown, A. Cassan, C. Cavarroc, A. Ciaravella, C. Cockell, A. Coustenis, C. Danielski, L. Decin, R. De Kok, O. Demangeon, P. Deroo, P. Doel, P. Drossart, L.N. Fletcher, M. Focardi, F. Forget, S. Fossey, P. Fouqué, J. Frith, M. Galand, P. Gaulme, J.I.G. Hernández, O. Grasset, D. Grassi, J.L. Grenfell, M.J. Griffin, C.A. Griffith, U. Grözing, M. Guedel, P. Guio, O. Hainaut, R. Hargreaves, P.H. Hauschildt, K. Heng, D. Heyrovsky, R. Hueso, P. Irwin, L. Kaltenegger, P. Kervella, D. Kipping, T.T. Koskinen, G. Kovács, A. La Barbera, H. Lammer, E. Lellouch, G. Leto, M. Lopez Morales, M.A. Lopez Valverde, M. Lopez-Puertas, C. Lovis, A. Maggio, J.P. Maillard, J. Maldonado Prado, J.B. Marquette, F.J. Martin-Torres, P. Maxted, S. Miller, S. Molinari, D. Montes, A. Moro-Martin, J.I. Moses, O. Mousis, N. Nguyen Tuong, R. Nelson, G.S. Orton, E. Pantin, E. Pascale, S. Pezzuto, D. Pinfield, E. Poretti, R. Prinja, L. Prisinzano, J.M. Rees, A. Reiners, B. Samuel, A. Sánchez-Lavega, J.S. Forcada, D. Sasselov, G. Savini, B. Sicardy, A. Smith, L. Stixrude, G. Strazzulla, J. Tennyson, M. Tessenyi, G. Vasisht, S. Vinatier, S. Viti, I. Waldmann, G.J. White, T. Widemann, R. Wordsworth, R. Yelle, Y. Yung, S.N. Yurchenko, *Experimental Astronomy* **34**, 311 (2012). DOI 10.1007/s10686-012-9303-4